LOCAL ILLUMINATION MODELS FROM SURFACE GEOMETRY

By

Gang Huo

B. Sc. Peking University

A THESIS SUBMITTED IN PARTIAL FULFILLMENT OF

THE REQUIREMENTS FOR THE DEGREE OF

MASTER OF SCIENCE

in

THE FACULTY OF GRADUATE STUDIES

COMPUTER SCIENCE

We accept this thesis as conforming

to the required standard

THE UNIVERSITY OF BRITISH COLUMBIA

April 1993

In presenting this thesis in partial fulfilment of the requirements for an advanced degree at the University of British Columbia, I agree that the Library shall make it freely available for reference and study. I further agree that permission for extensive copying of this thesis for scholarly purposes may be granted by the head of my department or by his or her representatives. It is understood that copying or publication of this thesis for financial gain shall not be allowed without my written permission.

(Signature)

Department of Computer Science

The University of British Columbia
Vancouver, Canada

Date April 27, 1993

Abstract

In this thesis, we propose a model to simulate the small-scale geometry of cloth and develop a method to derive the BRDF (Bidirectional Reflectance-Distribution Function) of this model from the underlying surface geometry, taking into account the blocking and shadowing phenomena at the small scale. Sample images of cloth generated with this BRDF look highly realistic. As a starting point to the inter-reflection problem, we examine the secondary reflection phenomena on the surface model made of parallel cylinders (as proposed by Poulin and Fournier) and the model proposed here for cloth. Two solutions are presented — sampling through raytracing and an analytical approximation. The results convincingly indicate that the intensity from multiply reflected light could be substantial for bumped surfaces with low specular exponent n. Therefore inter-reflection should be accounted for in the lighting model for these surfaces. Generated cloth images including secondary reflection effects exhibit a higher degree of realism. The computation of secondary reflection effects is however quite expensive.

The techniques presented can be extended to extract macroscopic reflection behaviour from the knowledge of the microscopic geometric structure.

Table of Contents

List of Tables

List of Figures

Acknowledgements

I am indebted to a number of people without whose advice and encouragement this work would not have been possible. Foremost on this list is Alain Fournier, who has supervised and contributed significantly to the development of this thesis. I am deepest grateful for the guidance, support, encouragement and solicitude that he has given me through my years at the University of British Columbia. His enthusiasm, approachability, inspiration, and generosity greatly helped produce the work presented here. I had the very good fortune to have studied under his supervision.

David Forsey, the second reader of my thesis, has spent a lot of time to review my early drafts, though he is himself very busy. I am truly grateful for his advices and suggestions which have substantially improved my thesis.

I would like to express my special gratitude to Pierre Poulin, whose work has had a deep impact on my own. Thanks give to him for generously taking the time to explain his early work, discuss and comment on my research. I am also very grateful to Chris Romanzin for reading early drafts of this thesis twice, offering helpful comments, as well as correcting language errors; John (Juancho) Buchanan for generously offering me code for numerical integration; Atjeng S. Gunawan and Robert Scharein for helpful discussions.

I would also like to extend my gratitude to all UBC graduate students, faculty, and staff who made my graduate study a rewarding experience, especially those in Imager/GraFic labs.

My family——my wife, our parents, my brother has been a constant source of inspiration and support, and I would especially like to acknowledge my wife Jun Zhang in this regard.

Chapter 1

Introduction and Previous Work

Calculating the shading of an object requires the computation of the intensity of the light reflected off the object and towards the viewer according to some illumination model. Correct shading is essential to achieving a high degree of realism. Improving the quality of the illumination model leads to direct improvements of realism. Phong [Phon73] introduced to computer graphics the first lighting model which went beyond the diffuse Lambertian shading model and included specular highlights. Blinn [Blin77] [Blin78] introduced and adapted the lighting models of Torrance and Sparrow [Torr67] and Trowbridge and Reitz [Trow75] to a form suitable for computer graphics. These were derived from a geometrical optics model for light reflection from surfaces. Cook and Torrance [Cook81] adapted these models and used a model based on [Beck63] that deals with the scattering of electromagnetic radiation from rough surfaces. Beckmann and Spizzichino's models [Beck63] do not make the same geometrical optics assumption. Wavelength dependence was a new factor in their work. All these led the way to well accepted and used illumination models. We can summarize their various formulations with a single equation:

$$\begin{aligned} I(\lambda) &= K_a(\lambda)S(\lambda)I_a(\lambda) \\ &\quad + K_d(\lambda)S(\lambda)\sum_{i=1}^{m}(\vec{N}\cdot\vec{L}_i)I_i(\lambda) \\ &\quad + K_s(\lambda)[(1-M(\lambda))S(\lambda)+M(\lambda)]\sum_{i=1}^{m}(\vec{N}\cdot\vec{H}_i)^n I_i(\lambda) \end{aligned} \tag{1.1}$$

where $K_a(\lambda)$, $K_d(\lambda)$, and $K_s(\lambda)$ represent respectively the proportion of light reflected in ambient, diffuse, and specular fashion, $S(\lambda)$ corresponds to the surface colour, $M(\lambda)$ the ratio metal/dielectric of the surface, n the surface specular exponent, $I_a(\lambda)$ the intensity of the ambient light and $I_i(\lambda)$ the intensity of each light source, $\vec{L}_i$ the direction to each light source (see figure 1.1), $\vec{N}$ the surface normal, and $\vec{H}_i$ the bisector of $\vec{E}$ and $\vec{L}_i$.

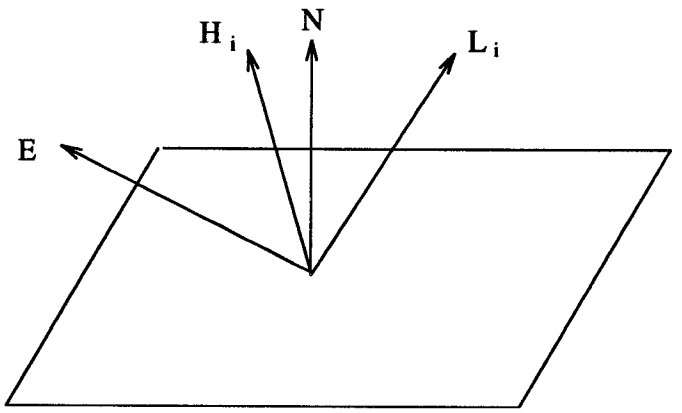

Figure 1.1: Vector Notation in Illumination Formulas

Several other parameters have been added to improve this simplistic model. Different roughness functions have been studied, geometric attenuations due to self-blocking have been taken into account and the Fresnel coefficient has been included for grazing angle effects. The same parameters controlling reflection have also been applied to refraction [Hall83] [Hall89].

Each of these improvements was justified as necessary in order to render scenes with a higher degree of realism. More recently, He et al. [He91] introduced a more accurate reflection model based on a more complete description of the surface characteristics. In order to derive such a comprehensive model, they introduced into their model several variables that capture certain previously neglected aspects of real reflection. Their model includes polarization of light, surface local height and slope, statistical connection of

surface asperities, and the concept of effective roughness. The model is based on physical optics and includes specular, directional diffuse, and uniform diffuse reflection from a surface.

To fully describe the characteristics of the light source, Gartaganis [Gart92] developed an illumination model that incorporates critical parameters related to the wave properties of light. This model describes the modification of optical disturbances that occurs when light is dispersed or diffracted. Gartaganis shows that this enhanced feature is crucial for successful duplication of some complex illumination effects such as dispersion and diffraction.

Looking realistic and being quickly computable are sufficient criteria for most lighting models used in raytracing systems. However, for the models used in radiosity systems, it is important to ensure that they satisfy the physical constraints of energy conservation and Helmholtz reciprocity. In [Lewi93], Lewis examined a number of lighting models commonly used in graphics in terms of the abovementioned criteria. His analysis shows that Torrance-Sparrow, Neumann-Neumann [Neum89] and Minnaert [Minn41] models conserve energy and satisfy reciprocity, while the Phong model fails on both counts. A modified Phong model is provided that is reciprocal and can be constrained to conserve energy.

These models reproduce many effects and are effective in simulating the reflection from surfaces with microscopic roughness, they can not model surfaces such as those with anisotropic roughness above the microscopic level. Aimed at such a common shortcoming, an alternate approach is to exploit specific details about the surface configuration to generate a more accurate BRDF (Bidirectional Reflectance-Distribution Function) model. Such models have been proposed by Kajiya [Kaji85], Cabral et al. [Cabr87], Poulin and Fournier [Poul89] [Poul90], Fournier [Four92], and more recently, Westin et al. [West92].

BRDF (Bidirectional Reflectance-Distribution Function) is sometimes used in computer graphics to describe the reflectance properties of an opaque surface element. To quote [ANS86], "*the Bidirectional Reflectance-Distribution Function f_r is the ratio of the differential luminance of a ray $dL_r(\theta_r, \phi_r)$ reflected in a given direction (θ_r, ϕ_r) to the differential luminous flux density $dE_i(\theta_i, \phi_i)$ incident from a given direction of incidence, (θ_i, ϕ_i) that produces it.*" (See figure 1.2)

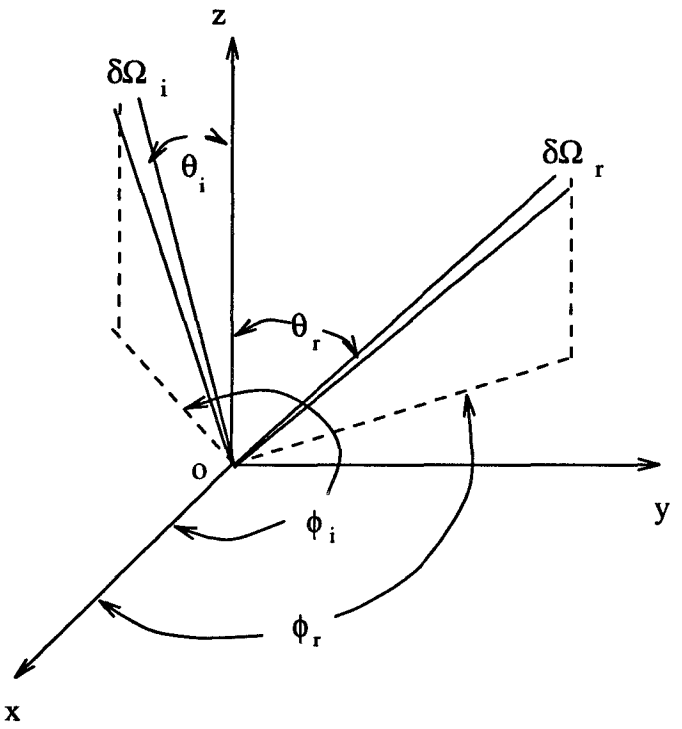

Figure 1.2: Definition of BRDF

$$f_r(\theta_i, \phi_i, \theta_r, \phi_r) \equiv dL_r(\theta_r, \phi_r)/dE_i(\theta_i, \phi_i) = dL_r(\theta_r, \phi_r)/L_i(\theta_i, \phi_i)d\Omega_i$$

where $d\Omega_i \equiv d\omega \cdot \cos\theta_i$.

In [Kaji85], Kajiya attempted to compute analytically the reflected intensity from a continuous surface. He based his approach on the general Kirchhoff solution for the scattering of electromagnetic waves [Bass79] [Beck63]. For given incident and reflected directions, the intensity reflected by a surface is computed. However, the method has its restrictions. For instance, the Kirchhoff solution is valid only if self-shadowing and multiple scattering are negligible. Even when this limitation is not considered, the size of the surface required (Fresnel zones) by the Kirchhoff solution and the stationary phase method used to approximate the integral [Born75] introduce new problems that are dependent on each surface type. Moreover, his method needs expensive preprocessing and a large memory.

Cabral et al. [Cabr87] start from the facet level. Facets are created from a height field and the reflection off each facet is studied, including the blocking factor for incident and reflected light. This method, which can be qualified as brute force, is computationally expensive. The computation of the blocking factor is done via a modification of Max's method for the self-shadowing of bump maps [Max88]. This method will seriously alias the shadows when used for surfaces that exhibit a high frequency behaviour. In these two approaches, the reflected intensities are computed once and stored in tables; interpolation between table entries is used for fast rendering. However, a new table needs to be computed for every type of surface and this computation involves a few hours of CPU time.

In [Poul89] [Poul90], Poulin and Fournier introduced a reflection and refraction model for anisotropic surfaces. The anisotropy is simulated by small parallel cylinders (added or subtracted from the base surface) distributed on the anisotropic surface. This corresponds to a "hidden" level between the micro-facet and macroscopic level. Different levels of anisotropy are achieved by varying the distance between each cylinder and/or raising the cylinders more or less from the surface. Their computation determines the

visible and illuminated portions of the cylinders first, taking self-shadowing, shadowing, self-blocking and blocking into account. Two techniques are presented to compute the intensity of reflected light. In one, the intensity is computed by sampling the surface of the cylinders and the other uses an analytical solution. For the diffuse term, the analytical solution is exact. For the specular term, an approximation is developed using Chebyshev polynomials and integrating them.

Fournier [Four92] introduces for local shading the concept of Normal Distribution Functions, or NDF for short. His motivation stems from the observation that, for many surfaces seen from a sufficient distance, the light reflected by a surface element is the result of reflection from a distribution of surface normals. Based on this observation, a normal distribution function for a surface is defined as a function that for each point on the surface gives the density of normals as a function of direction. This function can be used in traditional illumination models wherever the normal appears. By doing so, the BRDF is compactly represented and approximated. By treating the resulting surface as a multiple surface, i.e. one where each point has more than one normal, each normal contributes to the total reflectance. The technique allows simultaneous use of illumination models at different scales, ensuring smooth transition between scales when the scale changes. However, for some surfaces, the memory requirement of storing a NDF for each point on the surface would be very large. In practice, Fournier discretized the NDF and approximated it in several directions. The shading operation is just a sum of traditional operations. This might result in a loss of accuracy. Another problem is that it is difficult to take into account blocking and shadowing effects for normal distributions on non-convex surfaces. But they are approximated in the method.

Westin et al. [West92] described a Monte Carlo technique for approximating a BRDF by directly simulating optical scattering. They use spherical harmonics to represent the BRDF and store it in the form of a matrix of spherical harmonic coefficients. Using a

Monte Carlo technique, they estimate the coefficients of the representation by directly simulating optical scattering at a smaller scale. BRDFs for complex surfaces are simulated hierarchically by using the result of one simulation in generating the BRDF for the next larger scale. Their technique removes most restrictions on surface microgeometry and is therefore more general though still memory intensive. Even after reduction, the coefficient matrix of the spherical harmonics typically contains several thousands of elements. If the BRDF is sharper (i.e. the BRDF changes more sharply when the reflection direction varies.), the demand for storage could be expected to be much larger. For a scene with different scales of object detail, the storage required is almost intolerable. To estimate the coefficients by raytracing is very time consuming and the accuracy of the obtained result is questionable.

Another model was devised specifically for the reflection of cloth surfaces. In [Yasu92], T. Yasuda et al. attempted to establish a lighting model for cloth objects. This model implicitly inserts an intermediate level of facets between the macroscopic and microscopic level, corresponding to the scale of yarns. They assume the micro-facets composing each thread exhibits pure mirror reflection. Woven fabrics are made by interlacing two sets of yarns usually at right angles to each other (see figure 2.1). The lengthwise yarns are known as warp yarns, while the widthwise yarns are known as weft (or woof) yarns. At the intermediate level, the two groups of yarns (warps and wefts) are treated separately. They first experimentally measured the normal distribution function $\alpha(H)$ of one group of yarns over a small area. $\alpha(H)$ is the probability that a facet will have a normal in the direction of H. With the presence of the other group of yarns, the accuracy of the measured normal distribution function $\alpha(H)$ is questionable.

After obtaining experimentally $\alpha(H)$ and r_s, the weight of specular reflection, the specularly reflected intensity is computed as:

$$I_s = \alpha(H) \cdot r_s \cdot I_o$$

Here, I_o is the intensity of the incident light.

They also account for the light reflected or refracted several times at the border of internal fabric layers, namely *internal reflection.* Finally, they add some diffuse light to the reflected intensity:

$$I_d = I_o \cdot r_d \cdot (N \cdot L)$$

where I_o is the intensity of the incident light, r_d the experimentally measured weight of diffuse term, L the direction of the light source, N the global normal of the surface.

the reflected intensity from one group of yarns is calculated as the sum of the three components (specular, internal, and diffuse reflection). The reflection of the other group of yarns is calculated similarly. It seems that they rotate the previous measured $\alpha(H)$ such that it could be adapted as the normal distribution function of this group. They weighted the two components according to the ratio of warp and weft yarns appeared on the cloth surface, then simply sum them up as the final reflected intensity.

There are several problems and limitations in this approach. A fundamental assumption they make is that yarns are comprised of mirror-like facets. This is a very questionable assumption, since the gap between the scale of yarns and that of mirror-like facets is too large. There should be another level between them. This level should be characterized by Phong's or Blinn's lighting model but not a mirror-reflection model.

The model totally ignores the blocking phenomena which, as verified in [Tail92], is very important, especially for cloth surfaces, where the yarns may have very different sizes. When measuring the normal distribution function, as indicated in their paper [Yasu92], the technique is effective only for those weave patterns in which yarns in one direction dominates that of the other direction. This severely restricts the applicability of their method. More importantly, they transfer the normal distribution function of the

dominant group of yarns to the subordinate group[1], which is physically incorrect. They experimentally measured the relative weight of specular, internal and diffuse reflection with fixed lighting and viewing parameters, and then incorrectly assume that these ratios will remain unchanged under different viewing and lighting conditions. All these contribute to their somewhat unrealistic images.

[1]Woven fabric are composed by two sets of yarns. For some weave patterns, one can see more thread segments of one set per unit area than that of the other. This set of yarns is called the dominant group and the other set is called the subordinate group.

Chapter 2

Establishing the Surface Geometry

In establishing illumination models, one has to start with the surface geometry. It has been generally recognized that only in this way can the calculated BRDF accurately reflect the surface's optical behaviour. However, the application of this principle is not simple. One problem is that at the very beginning one has to properly identify the pixel level, that is, the level of detail that will be encompassed by a single pixel in the final image. Traditionally, it has been assumed that a two-level-partition is enough. That is, a microscopic level corresponding to the pixel level, and a macroscopic level corresponding to the large-scale visible geometry. This assumption is valid only if the viewer looks at the surface from a small distance or the surface of the object is very smooth. However, many scenes rendered nowadays in computer graphics are beyond this scope, and recently it has been realized in [Poul89] [Poul90] that two levels are not enough and that another level (called the *mesoscopic level* in [Four92]), corresponding to the pixel level, must be inserted between the microscopic and the macroscopic level. The underlying philosophy is that the eye is so far away relative to the dimension of the surface bumps[1] that a single pixel in the final image will include a small [2] region consisting of many surface bumps. Consequently, traditional lighting models are not valid for the reflectance off this small region, since those models are only for the micro-facets composing the surface bumps. Thus new models need to be constructed to accurately capture these situations.

Here we want to determine the reflected light off the cloth surface, and the situation

[1] In their approach [Poul89] [Poul90], the surface bumps are modeled as cylinders.

[2] yet very large compared to the surface bumps.

is very similar. We are interested in the case where the viewer and the light source are far away from the surface in comparison to the dimension Consequently, the individual thread can not be seen. by the eye. As such, the mesoscopic level corresponds to groups of threads, and the microscopic level corresponds to the facets consisting these threads. For these facets, we assume that they can be characterized by the traditional lighting models in computer graphics (e.g. Phong, Blinn). For groups of threads, the computation of their reflectance is a lot more complicated. In the remaining part of this chapter, we will elaborate first on the geometry of the mesoscopic level.

2.1 Threads

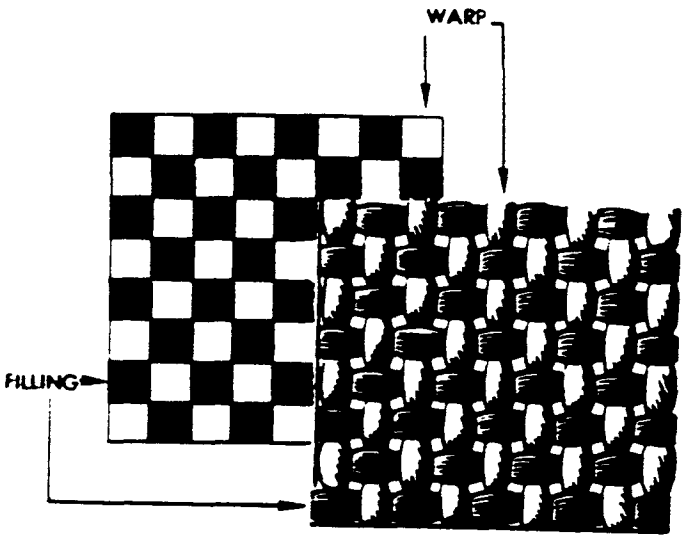

Figure 2.1: Woven Fabric
* taken from [Corb79], page 78, figure 5-6 (a).

As stated before, woven fabrics are made by interlacing two sets of yarns usually at right angles to each other (see figure 2.1). The lengthwise yarns are known as warp

yarns, while the widthwise yarns are known as weft (or woof) yarns. The cross-sectional shape of fibers exhibits some slight variations, but it is generally circular. Thus it is approximated with a semi-circle embedded into a plane (see figure 2.2). By adjusting the ratio of h and r, the cross-sections range from semi-circle to semi-ellipse. For some woven cloth, warps and wefts have different radii, and the warp (or weft) yarns are also composed of different kinds of threads with different radii. Accordingly, in our model, the mesoscopic level consists of two groups of cylinders corresponding to warp and weft yarns respectively. The orientation of the cylinders in one group is perpendicular to that of the other. The radii of the cylinders in different groups or even in a single group may not necessarily be the same.

It should be pointed out that our model is actually a simplification of the real geometry. We ignore the non-cylindrical parts of threads to simplify the computation. However, this might cause inaccuracy. But since the cylindrical parts are the dominant portion of the threads, the error will hopefully not be very much.

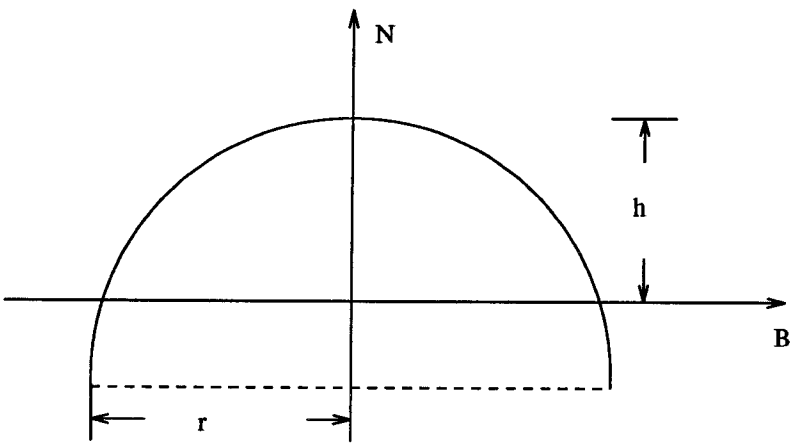

Figure 2.2: Approximation to the Cross-section of a Fiber

2.2 Weave Patterns

Depending on the direction of the light vector, one cylinder can block part of the light coming to another cylinder. This phenomena is called shadowing. Moreover, the cylinder can prevent part of itself from being lighted. This is called self-shadowing. Similarly, one cylinder can make part of another cylinder invisible to the viewer, called blocking; it can also make part of itself invisible, called self-blocking. For different weave patterns, the percentage of warps and wefts per unit area differs, and the shadowing and blocking scenarios also vary radically, resulting in very different reflection behaviours. In order to determine the BRDF accurately, we have to incorporate the weave pattern within our computation, since it is another very important aspect of surface geometry. To develop a general solution applicable to most of the encountered cloths, we have to look into what is common to the various weave patterns and is sufficient to characterizing the surface geometry.

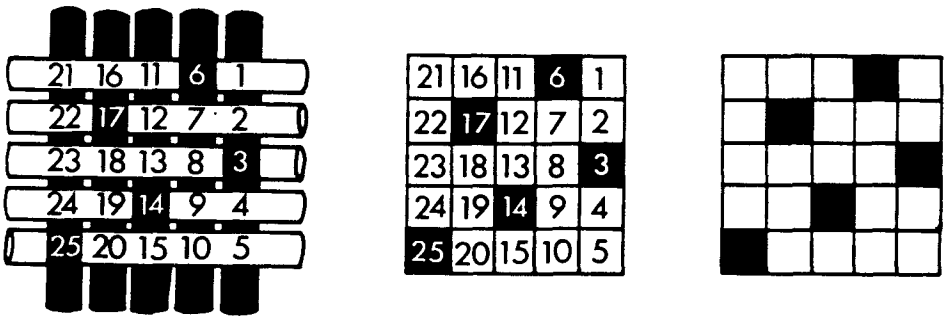

Figure 2.3: Weave Representation on Point Paper
* taken from [Pizz87], page 110, figure 4-9.

In Fabric Science, Point Paper (see figure 2.3) is used to show the weave or the order in which the yarns interlace in a fabric. It is used by textile designers to characterize a design. Each vertical row of squares represents a warp yarn and each horizontal row of squares represents a weft yarn. A warp crossing over a weft is usually shown by marking in the square. A blank square is used to show the weft yarn passing over the warp. For more knowledge about fabric science and textiles, consult [Corb79] [Pizz61] [Pizz87] [Tort87] [Wing84]. While it is sufficient to capture the entire surface constructions, Point Paper is still not the ultimate choice since the pattern might contain more than one period. By discarding redundancy, we can extract one period, which will be referred to as a weave period. For any given cloth, its weave pattern is completely determined by its weave period. Figure 2.4 shows a typical weave pattern, its Point Paper and its weave period.

2.3 Description of Surface Geometry

As stated before, our method will derive the BRDF of a surface from its geometry. For a cloth surface, two parameters are needed to specify the surface geometry: the weave period and relative dimension of the warp and weft yarns.

In our algorithm, the weave period is specified in the form of an array of binary 1's and 0's. A "1" corresponds to the marking in the weave period and "0" to the blank. As an illustration, the specification of the weave period in figure 2.4 is as follow:

```
1 0 1
1 1 0
0 1 1
```

Depending on the weave period, the size of the specification might be different.

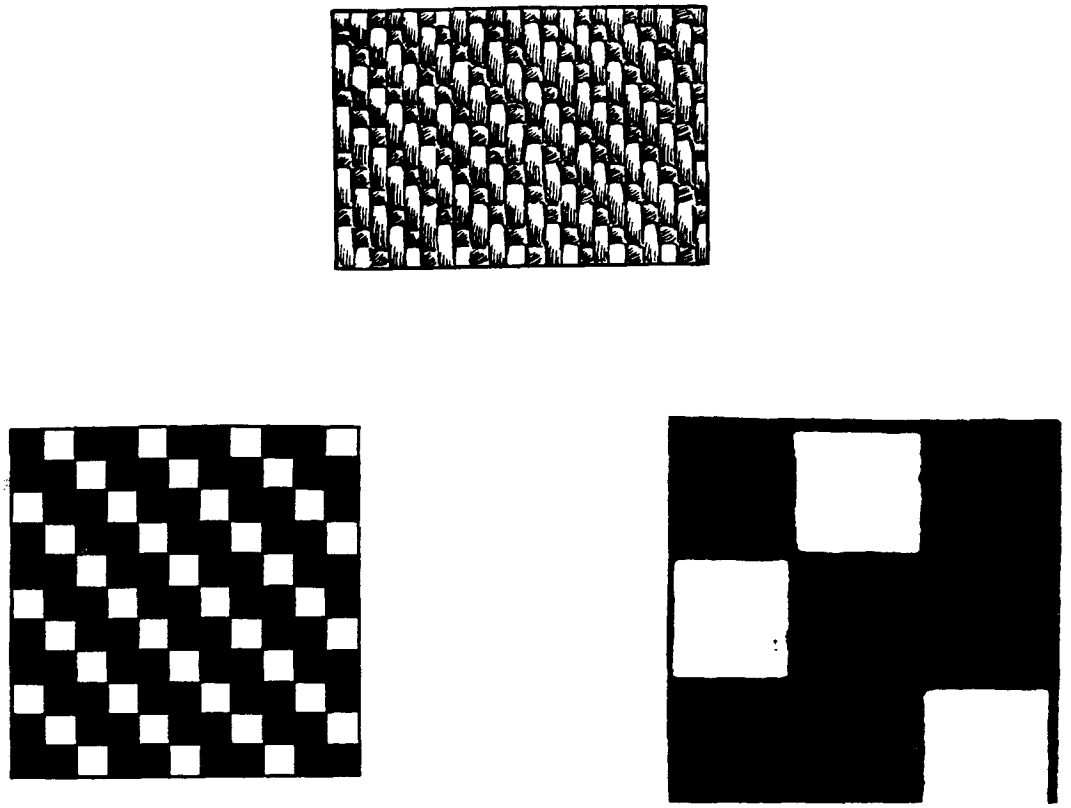

Figure 2.4: Weave Pattern & Point Paper & Weave Period
* taken from [Wing84], page 88, figure 4.12 (a) and (c).

The cylinders in different thread groups or even in a single group can be different. Therefore, we have to specify the radius and height of every thread in the weave period. In addition, the distances between adjacent warps (or wefts) may vary over the weave period. Therefore, the distance between every adjacent cylinder in each group must be provided. Later, we will see that this information about the weave pattern and the relative dimension of threads is sufficient and indispensable. From them, we can recover the relative positions of the thread segments so that we can determine the shadowing and blocking situations, and finally compute the reflected intensity from the surface.

Chapter 3

The Basic Geometry

This thesis addresses the specific case where the eye and the light source are far away from the cloth surface and therefore each displayed pixel will cover many weave periods. Because the distance from the eye to the surface is so large in comparison to the dimension of these weave periods, the direction of $\vec{E}$ is assumed to be constant over them. By the same token, $\vec{L}$ is also assumed constant over the weave periods embraced in a single pixel. Therefore, the light reflected from each weave period in this small region is the same. Thus the light reflected off a small region of cloth could be approximated by the reflectance of only one weave period in that region. For the units[1] in a weave period, because of their different orientations, or different kinds of neighbourhood, their blocking, shadowing, or reflection behaviours are different and must be counted individually. Furthermore, since $\vec{E}$ and $\vec{L}$ are identical over any thread segment in a weave period, its reflectance can be calculated as the reflectance off only one cross-section of the segment. Before going into the detail of the computation, we first examine the shadowing and blocking phenomena on the cloth surface.

3.1 Interactions Between the Thread Segments

The calculation of self-shadowing and self-blocking is the same as that appeared in [Poul89] [Poul90]. We will not repeat it here. Next we concentrate only on the interactions between the thread segments including shadowing and blocking.

[1] unit refers to a cylinder segment.

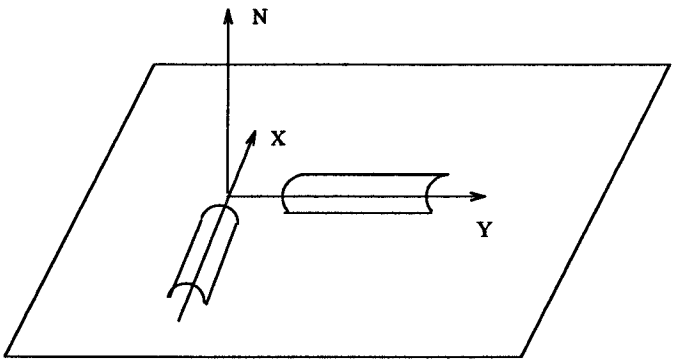

Figure 3.1: The Global Coordinate System

Figure 3.1 presents the global coordinate system. The X and Y axes are oriented along the directions of the threads. The local normals of the cylinders are either in the XN plane or the NY plane. The computations of shadowing and blocking are similar for the two groups of cylinders. Without loss of generality, here we only discuss the computation for the group of cylinder segments whose orientation is in the X axis direction.

The interactions between the thread segments can be categorized into three cases. We will examine each in detail. In the first case (figure 3.2), segment 2 shadows or blocks segment 1, depending on which vector we are considering. From the information of Point Paper, segment 3 does not influence segment 1. The influence of segment 4 on segment 1 is negligible, since in the shaded area, segment 4 is flattened out by segment 2, therefore it is too low to shadow or block segment 1. Another reason for ignoring the influence of segment 4 on segment 1 is that the length of the shaded part on segment 4 in figure 3.2 is not larger than the distance between two adjacent warps (or wefts). In most of the cases, it is very small relative to the radius of segment 2. To simplify the case further, we approximate the semi-circle (one cross-section of segment 2.) by an equal-area rectangle with length $2r_2$ (figure 3.3). This is reasonable since the viewer can only see the overall effect of shadowing and blocking. If r_2 is the radius of the semi-circle, the height of the

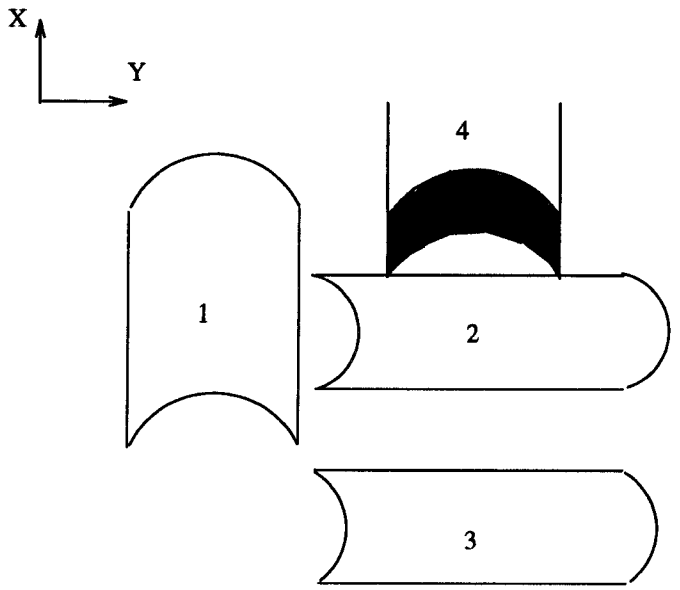

Figure 3.2: Interactions Between the Cylinders: the First Case

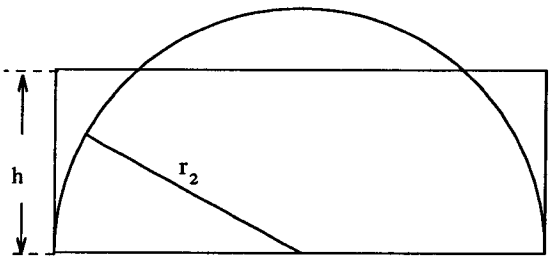

Figure 3.3: Approximation of Semi-Circle by Rectangle

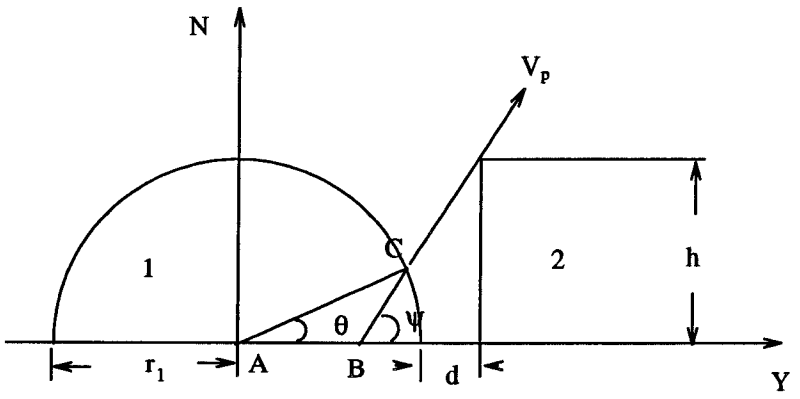

Figure 3.4: Cross-section of the First Case

rectangle is determined as :

$$h = \pi * r_2/4 \tag{3.1}$$

Figure 3.4 shows the projection of the two cylinders on the NY plane. One can see that segment 2 blocks part of segment 1 starting from angle 0 to θ. In $\triangle ABC$, we have:

$$\frac{\sin(\pi - \psi)}{\sin(\psi - \theta)} = \frac{r_1}{AB} \tag{3.2}$$

$$AB = r_1 + d - h/\tan\psi \tag{3.3}$$

combining 3.2 and 3.3, we can get:

$$\theta = \psi + \sin^{-1}\{\sin\psi/r_1 * [h/tan\psi - r_1 - d]\} \tag{3.4}$$

where r_1, r_2 are the radii of segment 1 and segment 2 respectively, d is the distance between the two cylinders, ψ is the angle between the Y axis and the projection of $\vec{V}$ on the NY plane[2].

For the second case (figure 3.5), segment 2 blocks segment 1. Figure 3.6 depicts the cross-section of the two cylinder segments. The blocking (or shadowing) angle θ can be computed from the following equation:

[2]The projection is denoted by $\vec{V}_p$ in figure 3.4. $\vec{V}$ could be $\vec{L}$ or $\vec{E}$.

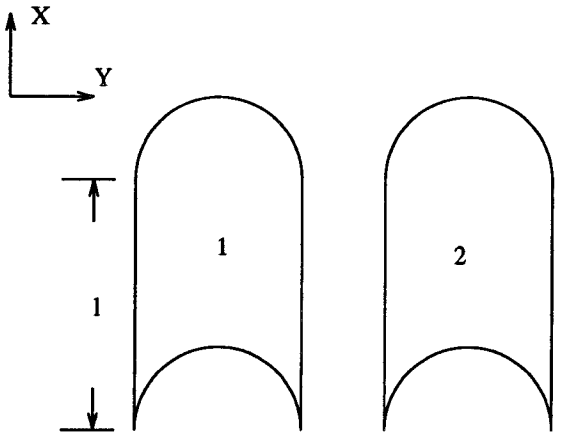

Figure 3.5: Interactions Between the Cylinders: the Second Case

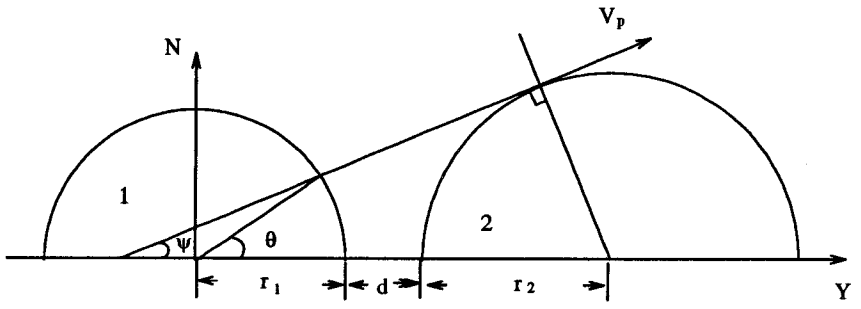

Figure 3.6: Cross-section of the Second Case

$$\theta = \psi + sin^{-1}(sin\psi/r_1 * (r_2/sin\psi - r_1 - d - r_2)) \tag{3.5}$$

where r_1, r_2, are the same as that appeared in equation 3.4, The meanings of the other symbols are depicted in figure 3.6.

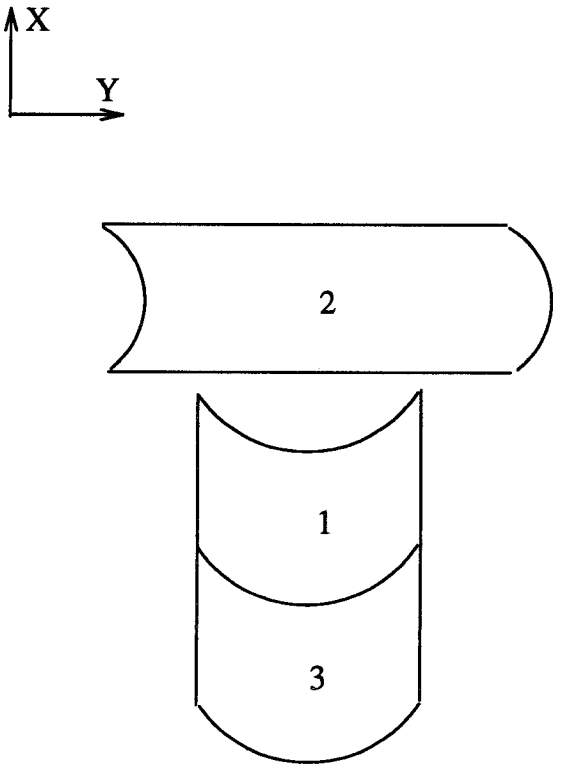

Figure 3.7: Interactions Between the Cylinders: the Third Case

The third interaction is depicted in Figure 3.7. Segment 2 blocks segment 1. Similar as for the first case, we approximate the cross-section of segment 1 by an equal-area rectangle so that the length of the shadow[3] that segment 2 casts on segment 1 is expressed as follows (figure 3.8):

$$l_s = (r_2 - h/\cos\psi)/\sin\psi - (d + r_2) + h\tan\psi \tag{3.6}$$

[3]or the length of the blocked part, depending on what $\vec{V}$ is.

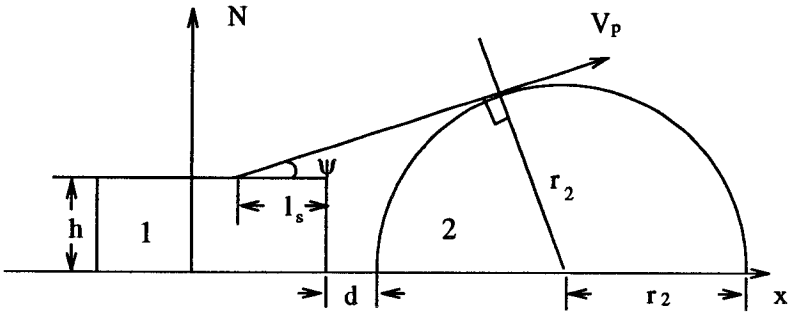

Figure 3.8: Cross-section of the Third Case

where

$$h = \pi * r_1/4$$

and the meanings of the other symbols are either the same as before or depicted in figure 3.8.

We have here only discussed the situations where the blocking cylinder is on the right or top of the blocked one. By symmetry same logic is applied to the cases where the blocking segment is on the left or below of the blocked one.

3.2 Range of Consideration

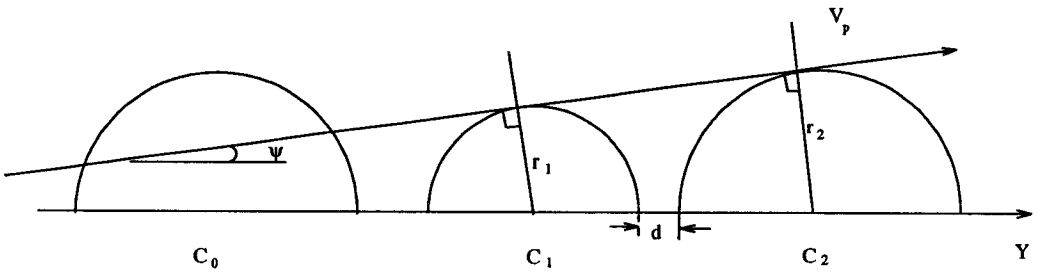

Figure 3.9: Range of Influence

The struggle with blocking is not yet over. In our model, because the radii of various cylinders in a weave period can be different, depending on the direction of $\vec{E}$ or $\vec{L}$ the segment actually blocking a certain cylinder may not be its immediately adjacent neighbour. For example, in figure 3.9, when the incident angle is less than ψ, segment 2 will actually influence segment 0 instead of segment 1. More generally, for any cylinder segment and different ranges of incident angle, the blocking cylinder can differ. For such a situation, we will preprocess the weave period so as to identify the "active" cylinders corresponding to different ranges of incident angle. For each of those units in a weave period with different radii or lengths, or different kinds of neighbourhood, we create four look-up tables, corresponding to its above, below, left and right directions. Table 3.1 illustrates the form of the tables. The look-up tables only depend on the weave pattern, not on $\vec{L}$ or $\vec{E}$, so this preprocessing procedure needs to be done only once for each given weave pattern. After establishing the look-up tables, given $\vec{L}$ and $\vec{E}$, we inspect the appropriate look-up table and find the corresponding "active" cylinder so that we can use the prototypes presented in the previous section to calculate the shadowing and blocking situations. Next we will present in detail the preprocessing procedure.

rangle of incident angle	active cylinder
$90 \sim \psi_1$	C_1
$\psi_1 \sim \psi_2$	C_2
$\vdots$	$\vdots$
$\vdots$	$\vdots$

Table 3.1: Look-up Table for One Direction

For each unit in a weave period with a unique set of parameters[4], we use a "cylinder scan" algorithm to establish the look-up table in each of four directions: above, below,

[4]include radius, height, length, neighbourhood

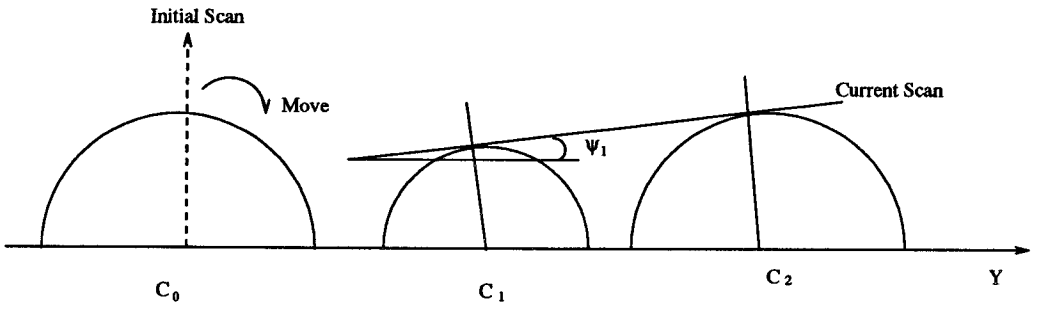

Figure 3.10: "Scanning the Cylinders"

left and right. The initial direction of the scan is perpendicular to the surface. Then we move the scan toward the floor (figure 3.10). The first cylinder segment met by the scan is C_1. Next we keep on moving the scan away from C_0 toward the horizon while it remains tangential to C_1 until it meets a new cylinder C_2. Suppose ψ_1 is the angle between the axis Y (or X) and the current scan, then C_1 will be the active segment while ψ, the incident angle of $\vec{L_p}$ or $\vec{E_p}$, is in the range of $[\psi_1, 90]$. We append the entry ψ_1 and C_1 to the look-up table. Next we continue to move the scan while it keeps tangential to C_2. The new cylinder encountered is denoted by C_3. The angle between the Y (or X) axis and the current scan is ψ_2. If $\psi_2 > 0$, then when the incident angle $\psi \in [\psi_2, \psi_1]$, the active cylinder will be C_2 accordingly. If, however, $\psi_2 \leq 0$, then when $\psi \in [0, \psi_1]$, the active cylinder will be C_2 and the algorithm stops immediately. This process will continue for C_3 similarly. The algorithm will stop once we have exhausted one weave period or the scan's incident angle reaches 0 degree. Next we will present the pseudocode of the algorithm. Figure 3.11 helps to understand the code. In figure 3.11, C_{i+n} is the repetition of C_i after one weave period. The pseudocode for the algorithm is as follows:

```
For each unit C[i] with independent parameters in a weave period
{
        j = i+1;
        repeat
```

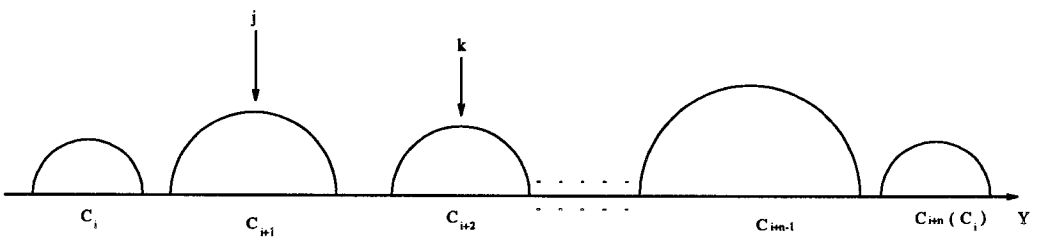

Figure 3.11: Graph for the Pseudocode

```
{
  k = j+1;
  MaxAngle = 0;
  /* find the first cylinder met by the scan tangential to C[j] */
  repeat
    {
       find the common tangent of C[j] and C[k];
       find the angle Psi from the common tangent to
       the Y (or X) axis;
       if (MaxAngle < Psi)
          {
            MaxAngle = Psi;
            MaxCylinder = C[k];
          }
       k++;
    } until ( k > i+n );
  if (MaxAngle > 0)
        /* when the incident angle is between MaxAngle and the
           angle in the previous table entry, then C[j] is the
           active cylinder */
       Append (MaxAngle, C[j]) to the table;
  else
    {
       /* when the incident angle is between the angle in the
          previous table entry and 0, then C[j] is the active
          cylinder, and the calculation for the current table
          finishes. */
       Append (0, C[j]) to the table;
       break;
    }
```

```
            /* next round should start with the MaxCylinder */
            j = index of MaxCylinder;
          } until ( j >= i+n)
}
```

The computation mainly involves finding the common tangent of two cylinder segments. This can be classified into three categories. For the first case (figure 3.9), ψ is determined by the following equation:

$$\psi = sin^{-1}((r_2 - r_1)/(r_2 + r_1 + d)) \tag{3.7}$$

where r_1, r_2 are the radii of segment 1 and segment 2 respectively.

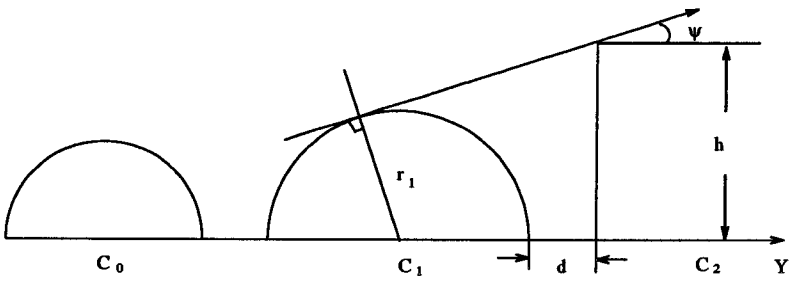

Figure 3.12: Active Cylinder Lookup Table Computation: case 2

For the second case (figure 3.12), ψ is determined by the following equations:

$$\begin{aligned} \psi &= \sin^{-1}((\sqrt{b^2 - 4ac} - b)/(2a)) \\ a &= r_1^2 + d^2 + 2r_1 d + h^2 \\ b &= 2r_1(r_1 + d) \\ c &= r_1^2 - h^2 \\ h &= \pi * r_2/4 \end{aligned} \tag{3.8}$$

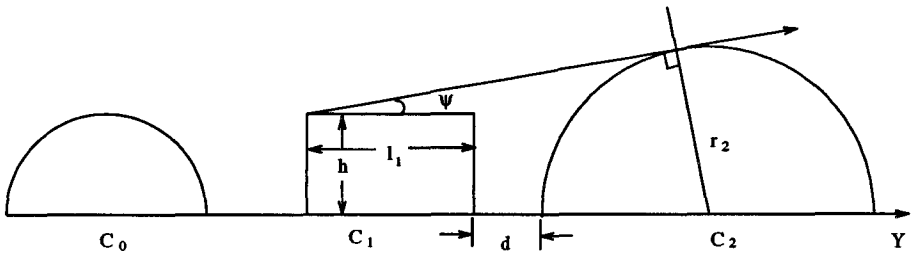

Figure 3.13: Active Cylinder Lookup Table Computation: case 3

For the third case (figure 3.13), ψ is determined by the following equations:

$$\begin{aligned} \psi &= \sin^{-1}((b - \sqrt{b^2 - 4ac})/(2a)) \\ a &= (l_1 + d + r_2)^2 + h^2 \\ b &= 2r_2(l_1 + d + r_2) \\ c &= r_2^2 - h^2 \\ h &= \pi * r_1/4 \end{aligned} \tag{3.9}$$

3.3 Summary

So far, we have presented the basic equations needed for the blocking and shadowing calculations. In summary, we first preprocess the weave period and establish look-up tables to determine the active cylinder. Then for some given $\vec{L}$ and $\vec{E}$, we query the proper look-up tables to find the corresponding active cylinders. Using the prototypes discussed in section 3.1, we can calculate the blocking and shadowing angles and lengths. In the next chapter, we will examine how to combine these results plus the angles from self-blocking and self-shadowing, and thereafter determine the visible and illuminated portion of cylinders. We will also present the computation of the final reflected intensity.

Chapter 4

Computation of Direct Reflected Light

In the previous two chapters, we elaborated on the surface geometry and the blocking phenomena. At this point, it should be clear how to calculate the blocking and shadowing angles and lengths for each "unit" in a weave period. This chapter examines the calculation of the directly reflected intensity. By directly we mean the light that is reflected only once by the surface towards the viewer. This computation is divided into three steps. Initially, determine the visible and illuminated portion of the cylinders and compute its projected area in the $\vec{E_p}$ direction; secondly, for each independent "unit" in a weave period, calculate the amount of light reflected from it; finally, sum up and average all these intensities. The projected areas computed at the beginning are used as weighting factors at the final step. We will now present each of these steps in detail.

4.1 Shadowing, Blocking and Computation of Projected Area

As detailed in the previous chapter, given $\vec{L}$ and $\vec{E}$, we use the look-up tables for each unit to determine the shadowing and blocking angles, and the lengths of the shadowed or the blocked part. Using the same calculation as in [Poul89] [Poul90], we can find the self-shadowing and self-blocking angles as well.

In general, two situations exist in the calculation of the visible and illuminated arc. Figure 4.1 depicts the first case. The length of the illuminated and visible cylinder (figure 4.2) can be calculated by the following code segment:

```
length_vi: length of visible and illuminated cylinder;
```

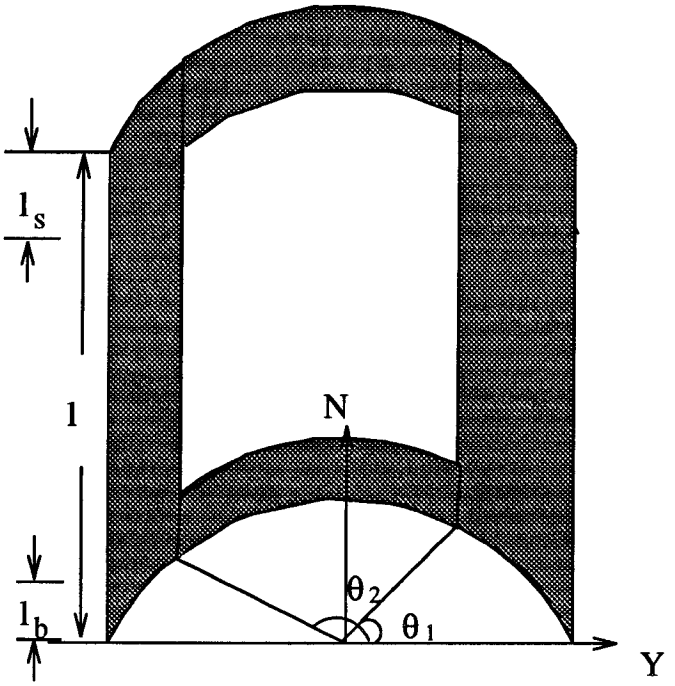

Figure 4.1: Visible and Illuminated Cylinder: Case 1

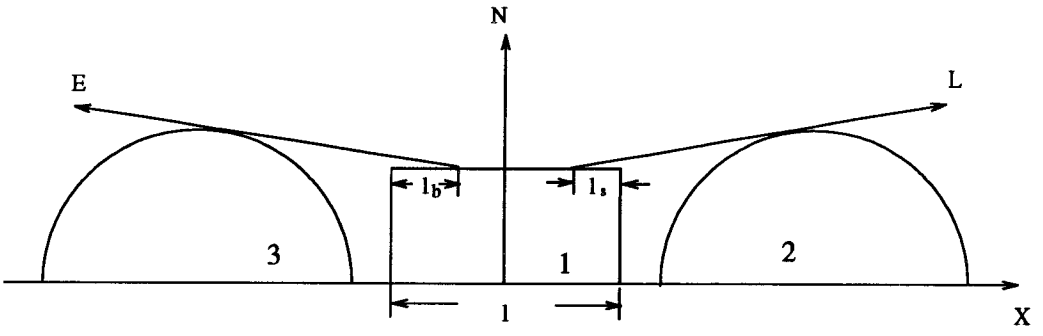

Figure 4.2: Length of Visible and Illuminated Cylinder

```
l_s:        length of shadowed cylinder;
l_b:        length of blocked cylinder;
l:          length of the cylinder segment;
if ( L and E on the same side of N when projected on to the XN plane)
     length_vi = Max(0, l-Max(l_s, l_b) );
else
     length_vi = Max(0, l-l_s-l_b);
```

Similarly, the length of visible cylinder is:

$$l_v = l - l_b \tag{4.1}$$

By combining the self-blocking, blocking, self-shadowing, shadowing angles, we can find the angles θ_1 and θ_2. The arc between $[\theta_1, \theta_2]$ is the illuminated and visible portion. In our computation of the final reflected intensity, we will need the projected area in the eye direction $\vec{E}_p$ of this visible and illuminated portion. We first need to find d_{vi}, the length of the arc when projected in the eye direction $\vec{E}_p$ (figure 4.3). It is determined as:

$$d_{vi} = r * (\sin(\theta_2 - \psi) - \sin(\theta_1 - \psi)) \tag{4.2}$$

Therefore, the projected area is

$$S_{vi} = l_{vi} * d_{vi} \tag{4.3}$$

where l_{vi} is the length of the visible and illuminated portion of the cylinder.

Figure 4.4 depicts the second case. For the portion of the cylinder between θ_2, θ_3, the calculation of the projected area in the $\vec{E}_p$ direction is the same as before, and we denote it as S_{vi1}.

For the portion of the cylinder between θ_1, θ_2, it is slightly more complicated. The length of the visible and illuminated portion is determined by the following code segment:

```
l_temp = (l-2*r3)/2;
if ( L and E are on the same side of N when projected on the XN plane)
   {
```

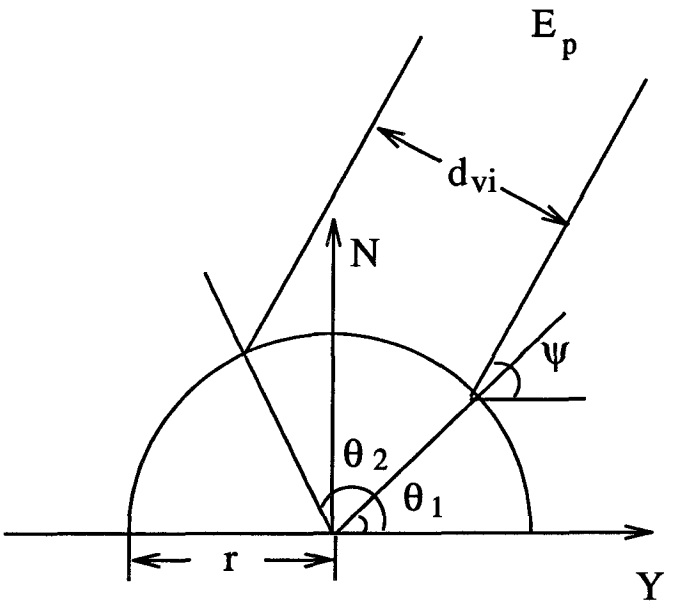

Figure 4.3: Length of the Arc Projected in the Eye Direction

```
    l_max = Max(l_s, l_b);
    if (l_max < l_temp)
       l_vi =  2*l_temp - l_max;
    else
       if (l_max < l_temp+2*r3)
          l_vi = l_temp;
       else
          l_vi = Max(0, l - l_max);
  }
else /* L and E are not on the same side of N */
    if ( (l_b > 2*r3+l_temp) or (l_s > 2*r3+l_temp) )
l_vi = Max(0, l - l_b - l_s);
    else
l_vi = Max(0, l_temp - l_b) +  Max(0, l_temp - l_s);
```

After obtaining l_{vi}, the calculation of the projected area is straightforward. we denote it as S_{vi2}.

A similar calculation can be applied to find the projected area in the $\vec{E}_p$ direction

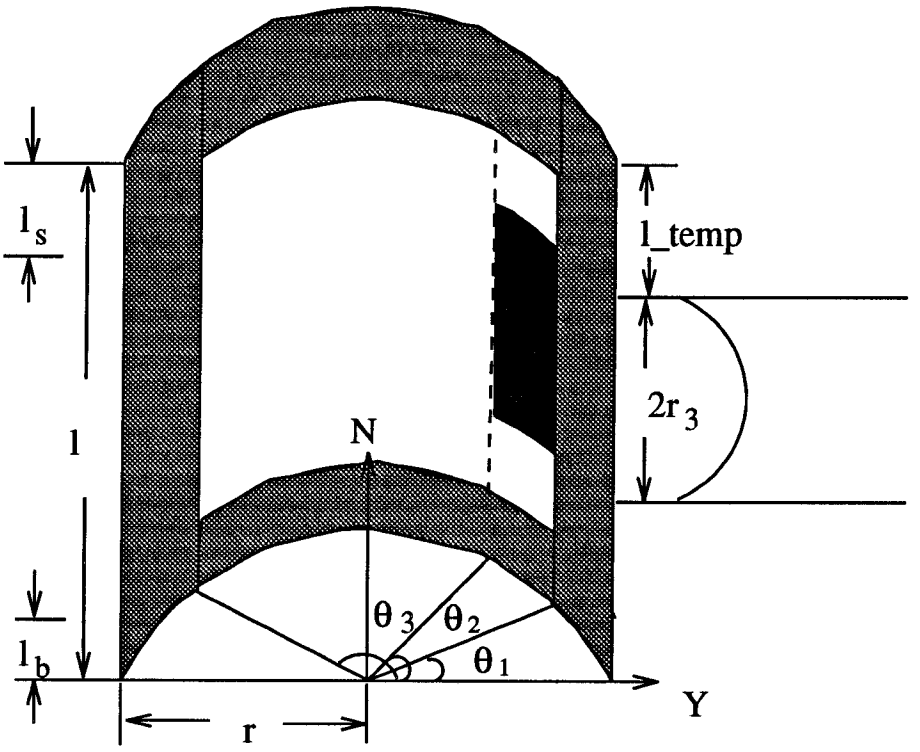

Figure 4.4: Visible and Illuminated Cylinder: Case 2

of the visible portion of a cylinder. We denote it as S_v, which will be used later in the computation of the final reflected intensity.

So far we have examined the group of cylinders oriented in the X axis direction. For the other group, the calculation is analogous.

4.2 Reflected Intensity

As stated before, since $\vec{L}$ and $\vec{E}$ are assumed constant over the numerous weave periods that will be embraced in a single pixel, the reflected intensity off this small region can be calculated as the reflectance off only one weave period. Furthermore, the reflectance off a thread segment can be computed as the reflectance off only one cross-section of the segment.

Reflectance off Individual Cylinder Segment

For thread segments, there are two cases in general. For the first case (figure 4.1), the reflected light is calculated as

$$I = \frac{S_{vi}}{S_v} \int_{\theta_1}^{\theta_2} (I_s + I_d) d\theta \tag{4.4}$$

where I_d, I_s are the diffuse and specular term respectively, S_{vi} is the visible and illuminated area when projected in $\vec{E}_p$ direction as given by equation 4.3, S_v is the sum of the projected areas in $\vec{E}_p$ direction of the visible portion of the cylinders over the weave period.

For the second case (figure 4.4),

$$I = \frac{S_{vi1}}{S_v} \int_{\theta_2}^{\theta_3} (I_s + I_d) d\theta + \frac{S_{vi2}}{S_v} \int_{\theta_1}^{\theta_2} (I_s + I_d) d\theta \tag{4.5}$$

where S_{vi1}, S_{vi2} are the projected areas in the $\vec{E}_p$ direction of the visible and illuminated portion of the cylinder between the arcs $[\theta_2, \theta_3]$, and $[\theta_1, \theta_2]$, respectively, the other symbols are the same as that in equation 4.4.

The terms $\frac{S_{vi}}{S}$ $\frac{S_{vi1}}{S}$, $\frac{S_{vi2}}{S}$ in equation 4.4 and 4.5 serve as weighting factors.
The term I_d in equations 4.4 and 4.5 is expressed as:

$$I_d = \vec{N} \cdot \vec{L} \tag{4.6}$$

Adding a correction factor $\cos(\theta - \theta_E)$ to the integrals in equations 4.4 and 4.5, we have:

$$\int I_d d\theta = \int \cos(\theta - \theta_E) \vec{N} \cdot \vec{L} d\theta \tag{4.7}$$

The term I_s in equations 4.4 and 4.5 is expressed as:

$$I_s = (\vec{N} \cdot \vec{H})^n \tag{4.8}$$

where, n is the surface specular exponent.

In this thesis, we use the phong-like model to characterize the micro-facets, since this model is well accepted in graphics. Other models can be easily used in our approach. We are concerned in this work about the reflection behaviours at the mesoscopic level and the comparison of the primary and the secondary reflection. As long as the micro-facet model is consistently used, our goals can be achieved.

Adding a correction factor $\cos(\theta - \theta_E)$ to the integrals in equations 4.4 and 4.5, we have:

$$\int I_s d\theta = \int (\vec{N} \cdot \vec{H})^n \cos(\theta - \theta_E) d\theta \tag{4.9}$$

The approximations and evaluations of equations 4.7 and 4.9 are discussed thoroughly in [Poul89] [Poul90]. We will not repeat it here. Obviously, due to the added correction factor, the solution obtained must be normalized by dividing by

$$\int_{\theta_1}^{\theta_2} \cos(\theta - \theta_E) d\theta = \cos\theta_E(\sin\theta_2 - \sin\theta_1) + \sin\theta_E(\cos\theta_2 - \cos\theta_1) \tag{4.10}$$

Total Reflected Intensity

Assume that in the weave period of a given cloth there are m independent "units". By independent, we mean the "units" have different radii, lengths, or neighbourhood[1]. Furthermore, for the ith "unit", there are D_i such instances in a weave period. Using the calculation we have just discussed, we can compute the intensity I_i reflected off a cylinder segment of the ith case. The total reflected intensity is then:

$$I = \sum_{i=1}^{m} D_i I_i \tag{4.11}$$

The pseudocode for the calculation is as follows:

```
I_total = S_total = 0.;
For each independent unit C[i] in the weave period
{
  if ( C[i] is case 1 (figure 4.2) )
     {
      calculate S_vi, the projected area of visible and illuminated portion;
      calculate S_v, the projected area of visible portion;
      evaluate the integral of the specular term: I_si;
      evaluate the integral of the diffuse term: I_di;
      I = S_vi * (I_si + I_di);
     }
  else /* C[i] is case 2 (figure 4.4) */
     {
      calculate S_vi1, S_vi2;
      calculate S_v;
      for part 1, evaluate the integral for I_si1, I_di1;
      for part 2, evaluate the integral for I_si2, I_di2;
      I = S_vi1 * (I_si1 + I_di1) + S_vi2 * (I_si2 + I_di2);
     }
  /* D[i] is the number of instances of case C[i] */
  S_total += S_v * D[i];  /* accumulate the visible areas */
  I_total += I* D[i];     /* accumulate the reflected intensities */
}
I_total /= S_total;      /* averaging */
```

4.3 Rendered Result

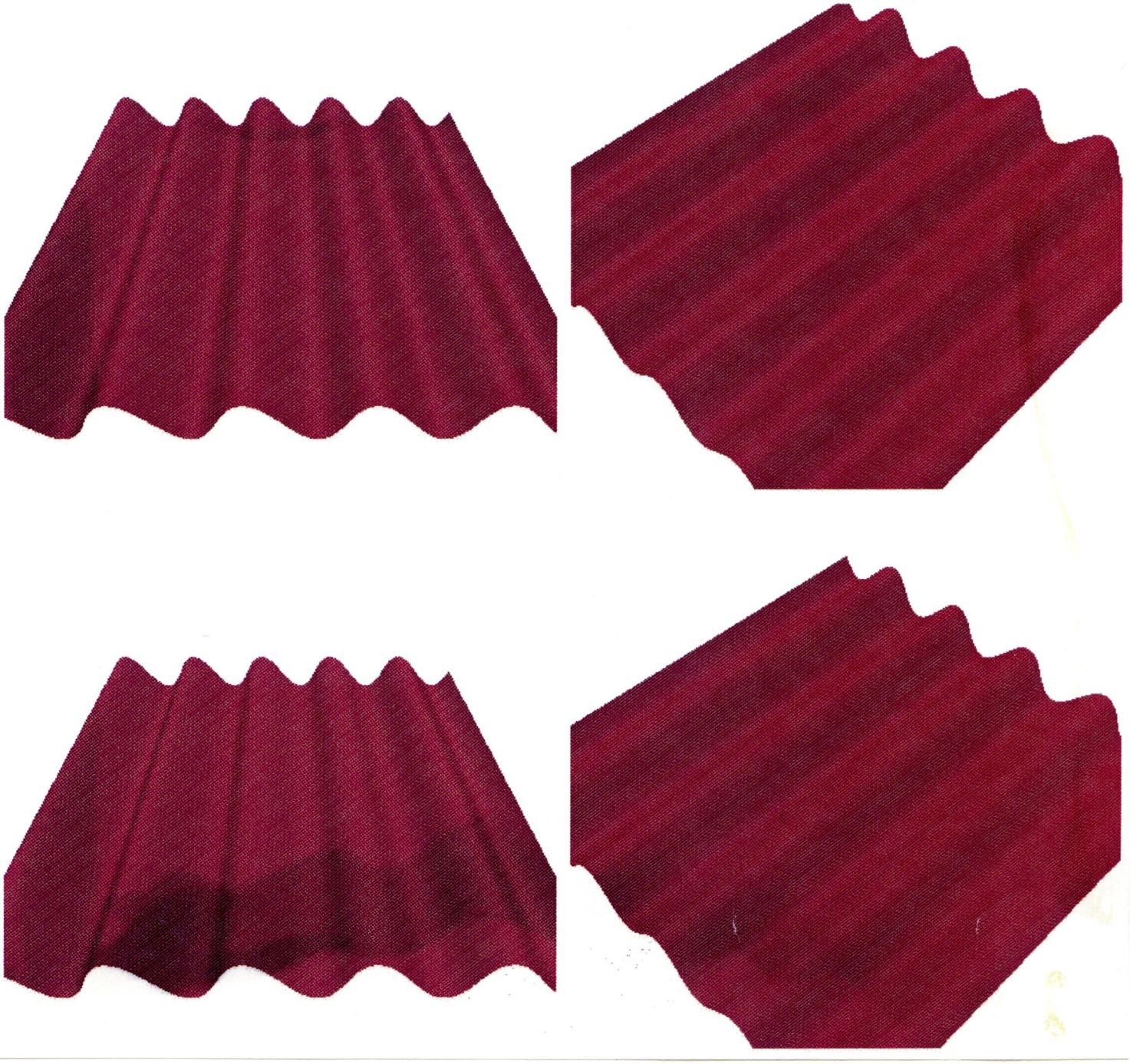

1	2
3	4

Image 1: basket weave (eye at (0, -55, 45)); Image 2: basket weave (eye at (-45, 45, 80));
Image 3: twill weave (eye at (0, -55, 45); Image 4: twill weave (eye at (-45, 45, 80)).

Figure 4.5: Sample Cloth Images

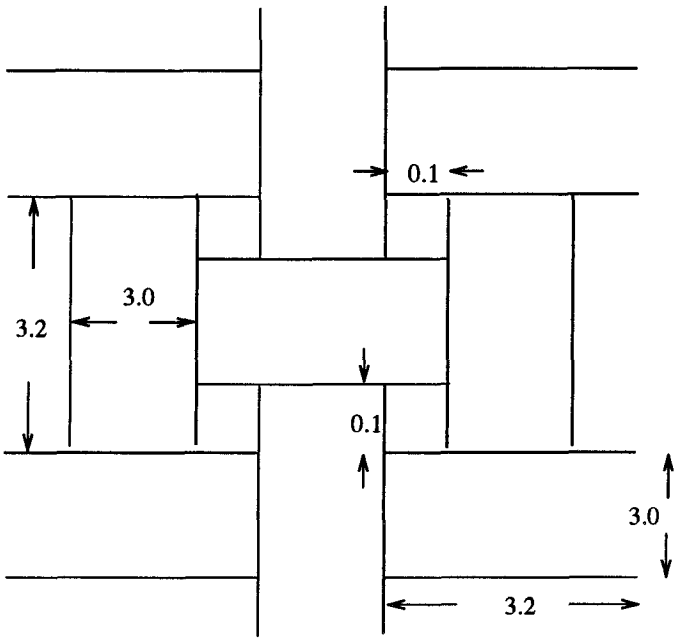

Figure 4.6: Surface Characterization of Sample Basket Weave

Figure 4.5 shows some images of cloth generated with this technique. For all four images, the surface is modelled by cubic spline resting on the average on the $Z = 0$ plane. In the figure, the upper two pictures are for a typical weave pattern, called "basket weave". Its weave pattern and some parameters used here are depicted in figure 4.6. The local surface geometry is characterized as two groups of cylinder segments perpendicular to each other. The radius of all cylinders is 1.5. The length of each cylinder segment is 3.2; the distance between two adjacent parallel cylinders is 3.1. The surface reflection parameters are specified as $\rho_a = 0.3$, $\rho_d = 0.4$, $\rho_s = 0.3$, $n = 10$. The directional light source is in the direction of (0, 0.707, 0.707). For the upper left image, the eye is at (0, -55, 45). For the upper right image, the eye is at (-45, 45, 80).

The lower two pictures in figure 4.5 are for another typical weave pattern, called

[1]Neighbourhood refers to the immediately adjacent units.

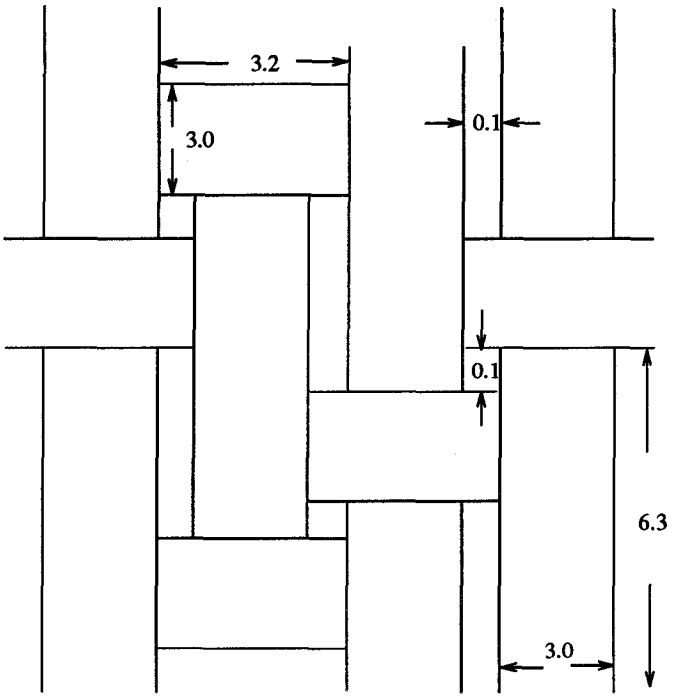

Figure 4.7: Surface Characterization of Sample Twill Weave

"twill weave". In these two pictures, the surface modelling, surface reflection parameters and light source are the same as those of the upper two pictures. The twill weave and some parameters used here are depicted in figure 4.7. For the local surface geometry, one group of cylinder segments has radius 1.5, length 6.3, the other has radius 1.5, length 3.2. The distance between two adjacent parallel cylinders is 3.1 for both directions. The eye position of the lower left picture is the same as that of the upper left one, and the eye position of the lower right picture is the same as that of the upper right one.

From the sample pictures, one can see that our approach is very successful. The images rendered using our algorithm look highly realistic. Comparing the images for the two different weave patterns, we are convinced that weave pattern is an important factor in determining the reflection behaviour. Therefore our algorithm have to be associated with weave pattern.

Regretfully, we lack the necessary equipment for measuring the reflectance properties of real cloth surfaces. Therefore, we can not yet compare the results with real data as a further verification of our approach. In addition, ρ_a, ρ_d, ρ_s and n are chosen empirically. Noticed that the weave patterns cannot be seen in the images. This is due to our assumption that the region embraced in a pixel is very large in comparison to the dimension of the weave period. Consequently, for different weave patterns, their difference is only perceived as different reflection behaviours. This is the limitation of our model.

Chapter 5

Inter-Reflection

Inter-reflection occurs when light reflects two or more times on a surface before it reaches the eye. Due to its complexity, this phenomena has not been dealt with quantitatively at a local scale in computer graphics. How important it is compared to direct reflection and blocking effects has yet to be determined. Traditionally, it has been taken for granted that this phenomena could be approximated by the diffuse term in lighting models. However, it is hard to tell how good this approximation is. It has been one of the continuous goals and trends in graphics to accurately capture the interaction between light and objects. As such, in order to achieve high degree of realism and be confident with our lighting model, we have to answer these questions, at least to some extent.

Secondary reflection, as indicated by its name, is when light is reflected two times at the surface before it comes to the eye (see figure 5.1). Obviously, the light reaching the eye via this process is the most significant portion of the multiply reflected intensity. Therefore, as a starting point to the inter-reflection problem, we will focus on the phenomena of secondary reflection in this chapter. The surface model under investigation is the anisotropic model proposed in [Poul89] [Poul90]. In what follows we will first briefly describe the surface model, then present two approaches to the solution——ray tracing and an analytical solution.

5.1 Geometric Model

Our primary concern here is at the mesoscopic level. As detailed in figure 5.1, at this level, the cylinders are embedded into a flat floor, r_1 and r_2 are the radii of cylinder C_1 and C_2 respectively and d is the distance between the centers of two adjacent cylinders. Some portion of the incoming light hits one cylinder C_2, reaches its adjacent cylinder C_1, and finally is reflected to the viewer. This is the phenomena of secondary reflection and is of our primary interest in this chapter.

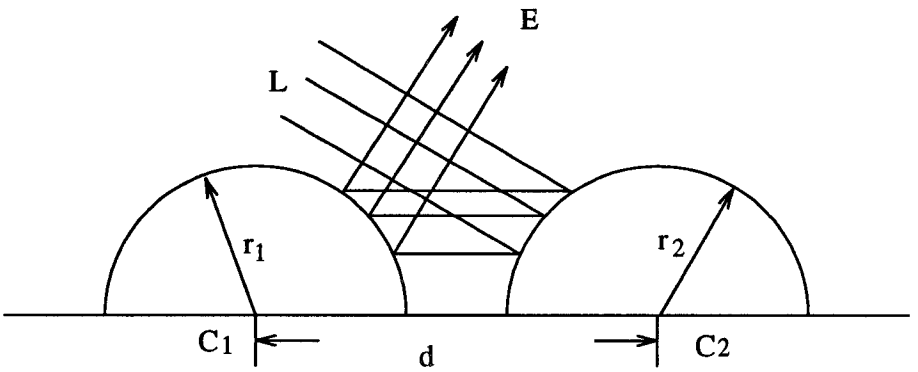

Figure 5.1: Secondary Reflection

5.2 Ray Tracing Solution

In spite of the computational cost required, raytracing is usually an effective technique to simulate the interaction between light and objects. In this section we will present the sampling schemes.

5.2.1 First Level Sampling Scheme

We use the sampling scheme presented in [Poul89] [Poul90] as our first level scheme, that is, sampling the cylinder at regular intervals as seen by the viewer (see figure 5.2). We

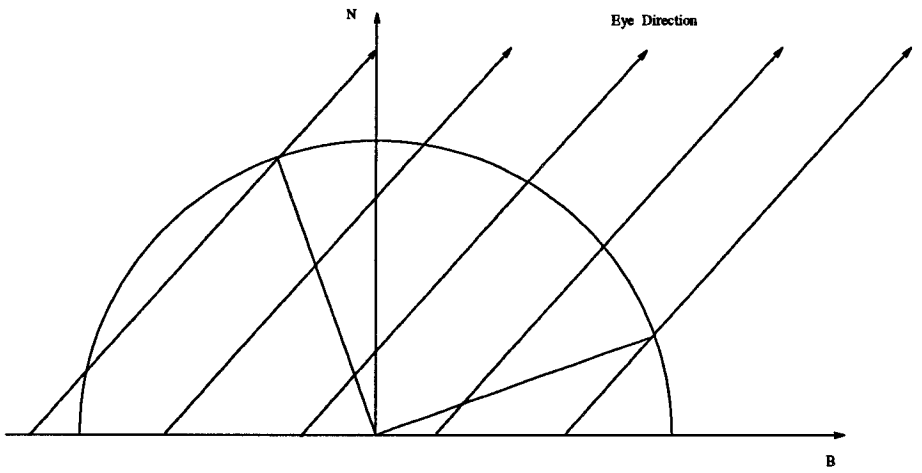

Figure 5.2: Sampling as Seen by the Viewer

first identify the sampling positions and their normals on the visible arc. Then for each of these positions, we calculate the intensity I_i reflected via secondary reflection from this point to the eye. The final reflected intensity to the viewer is the average of all these intensities I_i from each sampling position (equation 5.1.)

$$I = \frac{1}{n}\sum_{i=1}^{n} I_i \tag{5.1}$$

where n is the number of samples on each cross-section of the cylinder.

5.2.2 Second Level Sampling Scheme

To calculate the abovementioned I_i, the intensity reflected from position P_i to the viewer, we have to sample the area that is visible to P_i and illuminated by the light source on its adjacent cylinder C_2 (see figure 5.3).

The determination of this area is slightly more involved. Along the y axis direction, the length considered is decided by the user, taking distance attenuation into account. Normally, a range of $[-1.5, 1.5]$ for a cylinder radius of 1.0 is sufficient for a visually good

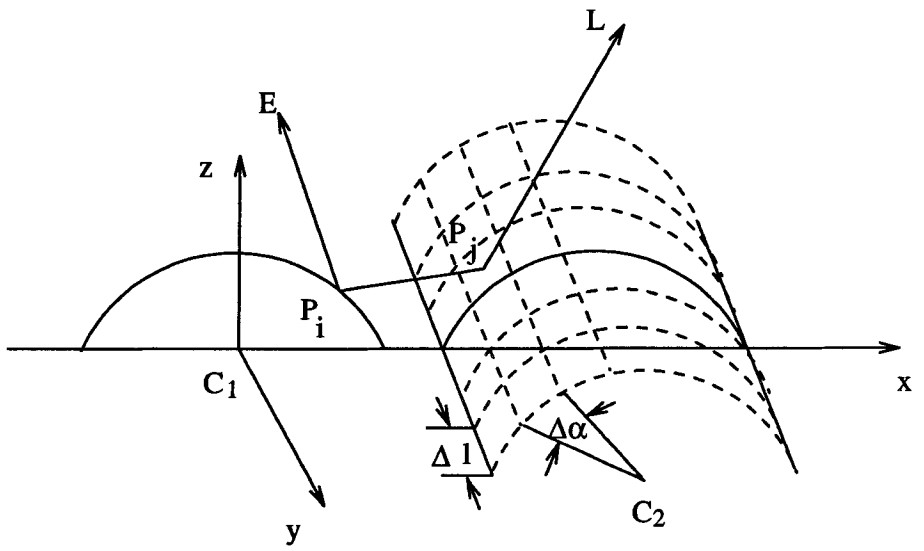

Figure 5.3: Second Level Sampling

image. However, for each cross-section we have to compute the arc which is visible to P_i and illuminated by the light source. In figure 5.4, we suppose that the arc P_uP_l on C_2 is visible to P_i on cylinder C_1. θ_u and θ_l are the angles measured from the z axis to O_2P_u and O_2P_l respectively. These angles are calculated as follows.

In figure 5.4, line P_iP_u is tangent to circle C_2. Its equation is:

$$(x_u - d)(x - d) + z_u z = r_2^2 \tag{5.2}$$

where (x_u, z_u) is P_u's coordinate, r_2 is the radius of cylinder C_2, d the distance between the centers of the two cylinders.

Also we know P_u's coordinate is $(d - r_2 \sin\theta_u, r_2 \cos\theta_u)$, P_i's is $(r_1 \sin\phi, r_1 \cos\phi)$, and P_i is on the line P_iP_u. Here r_1 is the radius of circle C_1. Therefore we have the following equation:

$$(d - r_2 \sin\theta_u - d)(r_1 \sin\phi - d) + r_2 r_1 \cos\theta_u \cos\phi = r_2^2 \tag{5.3}$$

For P_i on the other side of the x axis, the equation is the same. By solving equation 5.3, θ_u is computed as follows:

$$\begin{aligned} k_1 &= d - r_1 \sin(\phi); \\ k_2 &= r_1 \cos(\phi); \\ \theta_u &= \arcsin(\frac{r_2 * k_1 - k_2 * (k_1^2 + k_2^2 - r_2^2)^{1/2}}{k_1^2 + k_2^2}); \end{aligned} \tag{5.4}$$

Similarly, line P_iP_l is tangent to circle C_1. Its equation is:

$$x_i x + z_i z = r_1^2 \tag{5.5}$$

where (x_i, z_i) is P_i's coordinate, r_1 is the radius of cylinder C_1. Also since P_i's coordinate is $(r_1 \sin\phi, r_1 \cos\phi)$, P_u's is $(d - r_2 \sin\theta_l, r_2 \cos\theta_l)$, P_l is on the line P_iP_l, we have the following equation:

$$r_1 \sin\phi(d - r_2 \sin\theta_l) + r_1 r_2 \cos\phi \cos\theta_l = r_1^2 \tag{5.6}$$

For P_i on the other side of the x axis, the equation is the same. By solving equation 5.6, θ_l is computed as follows:

$$\theta_l = \arccos(\frac{r_1 - d * \sin\phi}{r_2}) - \phi; \tag{5.7}$$

The above computation can be summarized as:

$$\begin{aligned} k_1 &= d - r_1 \sin(\phi); \\ k_2 &= r_1 \cos(\phi); \\ \theta_u &= \arcsin(\frac{r_2 * k_1 - k_2 * (k_1^2 + k_2^2 - r_2^2)^{1/2}}{k_1^2 + k_2^2}); \\ \theta_l &= \arccos(\frac{r_1 - d * \sin\phi}{r_2}) - \phi; \end{aligned} \tag{5.8}$$

where r_1 is the radius of cylinder C_1, r_2 is the radius of cylinder C_2, d the distance between the centers of the two cylinders, ϕ is the angle between O_1P_i and the z axis.

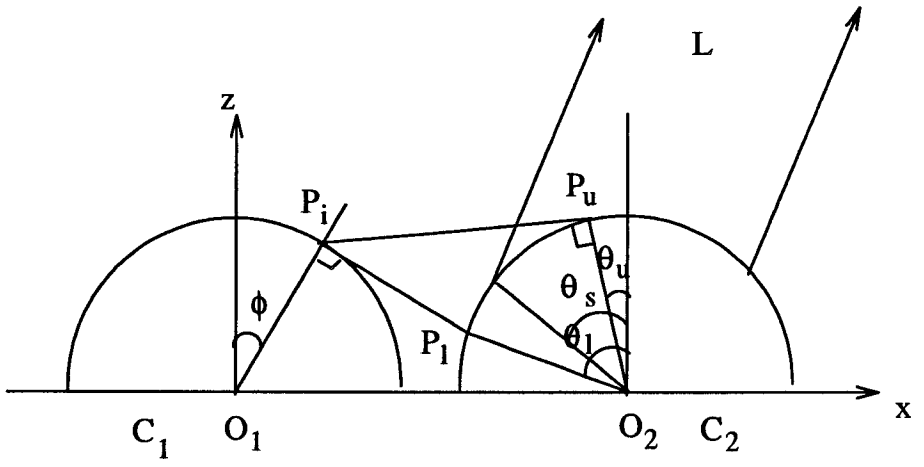

Figure 5.4: Determination of Sampling Range on Adjacent Cylinder

With the two angles θ_u and θ_l, and the shadowing angle θ_s from the light source, the sampling range on one cross-section of C_2 is determined to be from θ_u to $min(\theta_l, \theta_s)$.

After finding this range, we sample it regularly as shown in figure 5.3. For each cross-section, we divide it by a constant interval $\Delta\alpha$; along the y axis, we divide the cylinder by a constant interval Δl. Normally, $\Delta\alpha = 0.2, \Delta l = 0.2$ will give very good result. For each of these patches, we shoot a ray to its center P_j. The light reflected from P_j to P_i and finally to the viewer has two reflections on its way. Therefore, the light reflected in this way has four components: light reflected specularly at the two reflections whose intensity will be referred to as I_{ss_i}; light first reflected specularly and then diffusely, I_{sd_i}; light first reflected diffusely and then specularly, I_{ds_i}; and light reflected twice diffusely, I_{dd_i}. For I_{ss_i},

$$I_{ss_i} = \sum_j \rho_s I_{ji} (\vec{N}_i \cdot \vec{H}_i)^n (\vec{N}_i \cdot \vec{P_iP_j}) d\omega_{ij} \tag{5.9}$$

where ρ_s is the specular-reflection coefficient, I_{ji} is the intensity reflected from P_j to P_i, $\vec{P_iP_j}$ is the unit vector from P_i to P_j, $\vec{N}_i$ is the normal at P_i, $\vec{H}_i$ is the bisector of $\vec{E}$ and $\vec{P_iP_j}$, $d\omega_{ij}$ is the solid angle of patch j with respect to P_i.

The term I_{ij} in the above equation is:

$$I_{ij} = \rho_s(\vec{N_j} \cdot \vec{H_j})^n \tag{5.10}$$

where $\vec{N_j}$ the normal at P_j, $\vec{H_j}$ the bisector of $\vec{L}$ and $\vec{P_jP_i}$.

Combining equations 5.9 and 5.10 we have:

$$I_{ss_i} = \rho_s^2 \sum_j (\vec{N_i} \cdot \vec{H_i})^n (\vec{N_j} \cdot \vec{H_j})^n (\vec{N_i} \cdot \vec{P_iP_j}) d\omega_{ij} \tag{5.11}$$

Similarly, we have:

$$I_{sd_i} = \rho_s \rho_d \sum_j (\vec{N_i} \cdot \vec{P_iP_j})(\vec{N_j} \cdot \vec{H_j})^n (\vec{N_i} \cdot \vec{P_iP_j}) d\omega_{ij} \tag{5.12}$$

$$I_{ds_i} = \rho_s \rho_d \sum_j (\vec{N_i} \cdot \vec{H_i})^n (\vec{N_j} \cdot \vec{L})(\vec{N_i} \cdot \vec{P_iP_j}) d\omega_{ij} \tag{5.13}$$

$$I_{dd_i} = \rho_d^2 \sum_j (\vec{N_i} \cdot \vec{P_iP_j})(\vec{N_j} \cdot \vec{L})(\vec{N_i} \cdot \vec{P_iP_j}) d\omega_{ij} \tag{5.14}$$

$$I_i = I_{ss_i} + I_{sd_i} + I_{ds_i} + I_{dd_i} \tag{5.15}$$

where ρ_d is the diffuse reflection coefficient.

To compute the term $(\vec{N_i} \cdot \vec{P_iP_j}) d\omega_{ij}$ in the above equations, Siegel et. al. have shown [Sieg81] that it is equivalent to projecting patch j onto a unit hemisphere centered about P_i and projecting this projected area orthographically down onto the hemisphere's unit circle base. Here we use this method for its accuracy. Alternatives exist. If we discretize the patches finely enough, the solid angle can be approximated as the patch's foreshortened surface area divided by the square of the distance from P_j to P_i. Foreshortened surface area, also known as projected surface area, refers to the projection of patch j onto the plane perpendicular to $\vec{P_iP_j}$. Accordingly, the solid angle can also be approximated as:

$$d\omega_i \approx \frac{(\vec{N_j} \cdot \vec{P_jP_i}) dA_j}{R^2} \tag{5.16}$$

where $\vec{N_j}$ the normal at P_j, $\vec{P_iP_j}$ the unit vector from P_j to P_i, dA_j the area of patch j and R the distance from P_j to P_i.

5.3 Analytical Solution

To compute the secondary reflection analytically, we first have to realize several facts. In the surface model proposed in [Poul89] [Poul90], for each cylinder, given $\vec{L}$ and $\vec{E}$, on each side of the z axis, there exists at most one point P_1 on C_1, such that: there exists a line on its adjacent cylinder C_2; for any point (say P_2) on this line, light ray hits P_2, then reaches P_1, then is reflected to the viewer; the two reflections on this path when projected onto the xz plane are all pure mirror reflections. Figure 5.5 depicts this situation. We call P_1 the *maximum reflection point* and the special line on cylinder C_2 *peak line.* From the definition of the peak line we can know it is parallel to the y axis.

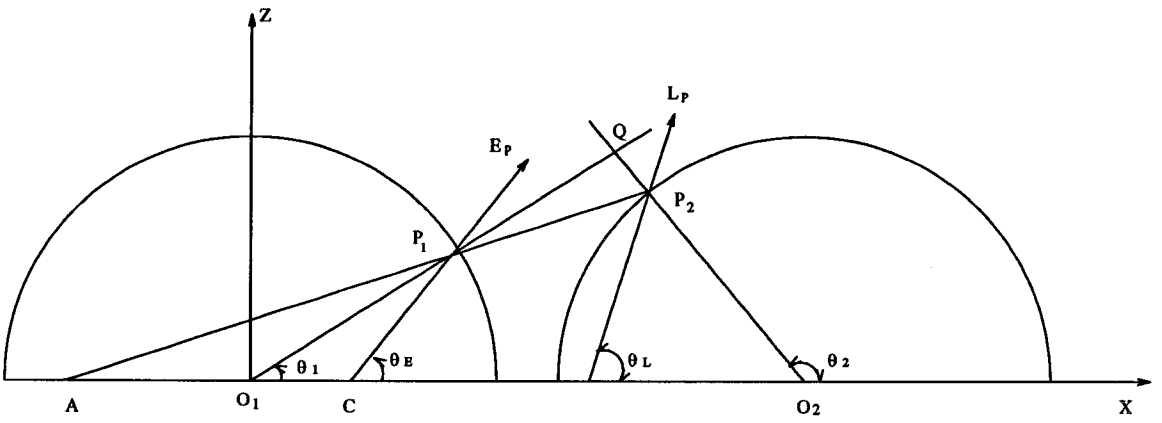

Figure 5.5: Maximum Reflection Point and Peak Line Determination

Due to the curvature of the cylinder, the contribution of the secondary reflected intensity drops dramatically for those positions slightly offset from P_1 or the peak line. The regions surrounding P_1 and the peak line contribute the most to the secondary reflection. Thus in our analytical solution we only need to consider these regions. Next we will describe how to determine the maximum reflection point and the peak line.

5.3.1 Maximum Reflection Point and Peak Line Determination

In figure 5.5, $\vec{E_p}$ and $\vec{L_p}$ are the projections of $\vec{E}$ and $\vec{L}$ on the XZ plane, respectively. P_1 is the maximum reflection point, while P_2 is a point on the peak line with same y coordinate as P_1. Our goal in determining the peak line is to compute the angle from the x axis to O_2P_2, θ_2 in figure 5.5. To determine the maximum reflection point P_1 we must compute the angle θ_1 in figure 5.5. Consider the triangles $\triangle O_1O_2Q$ and $\triangle P_1P_2Q$, we have

$$\theta_2 - \theta_1 = \pi - (\theta_E - \theta_1) - (\theta_2 - \theta_L) \tag{5.17}$$

From equation 5.17, we can get

$$\theta_2 - \theta_1 = \pi/2 + \frac{\theta_L - \theta_E}{2} \tag{5.18}$$

The coordinate of P_1 is $(r_1 \cos\theta_1, r_1 \sin\theta_1)$, and P_2 's is $(d+r_2 \cos\theta_2, r_2 \sin\theta_2)$. Considering $\triangle ACP_1$, the angle between P_1P_2 and the x axis is $\theta_E - 2(\theta_E - \theta_1)$ (i.e. $2\theta_1 - \theta_E$). Hence we have equation

$$\frac{r_2 \sin\theta_2 - r_1 \sin\theta_1}{d + r_2 \cos\theta_2 - r_1 s \cos\theta_1} = \tan(2\theta_1 - \theta_E) \tag{5.19}$$

The combination of equation 5.18 and 5.19 results in a four-degree polynomial equation. By solving it and finding out the correct answer, we can determine θ_1 and θ_2. For the case that the points are on either side of the z axis, the equations are the same.

5.3.2 Formula for Secondary Reflection

From the underlying assumption about the surface model (i.e. the scale of cylinders is very small compared to eye and light source), the intensity reflected by all the cylinders can be calculated as the reflection from a single cylinder[1]. Furthermore, since the radius of

[1]This is true only if the radii of the cylinders are the same. If, however, this is not the case, we have to compute the reflected intensities for each kind of cylinder with different radii, then average them weighted by the projected area in the eye direction of the visible cylinder. The rest of the computation is the same as presented next.

a cylinder is very small in comparison to its length, the intensity reflected from a cylinder can be approximated by the reflection off only one cross-section of it. For each cylinder, the viewer position is so far away relative to the cylinder's radius that its direction can be assumed to be constant over the cylinder. By the same token, the light direction is also assumed constant over each cylinder.

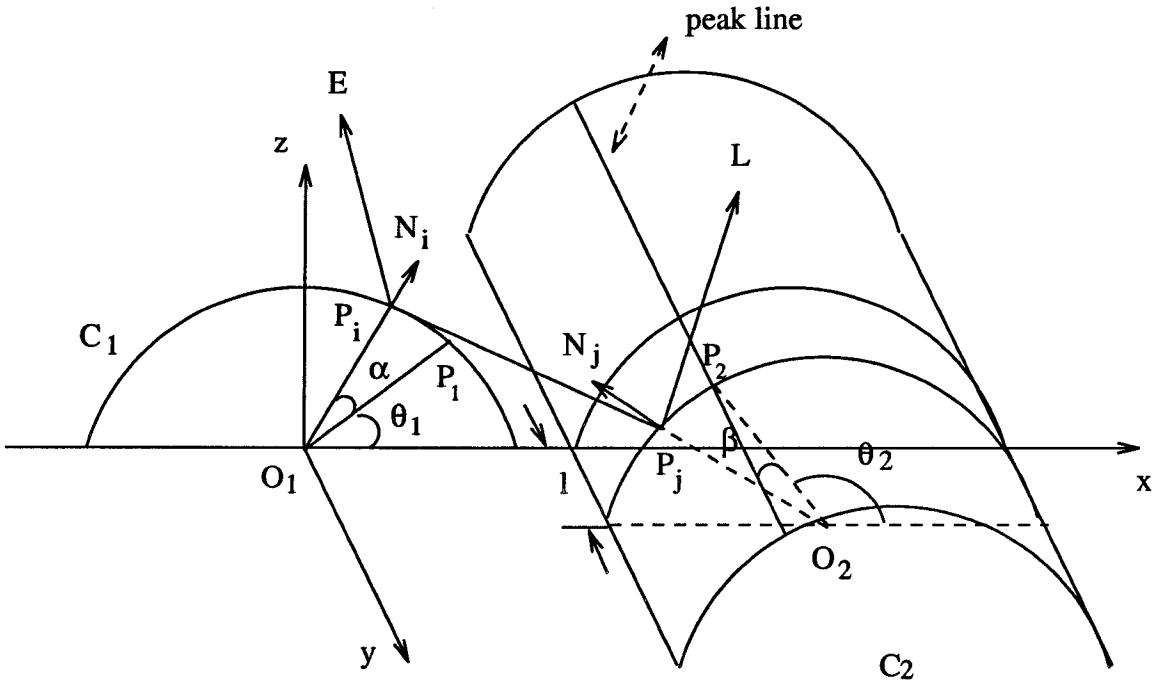

Figure 5.6: Integration for Secondary Reflection

In figure 5.6, P_1 is the maximum reflection point and P_2 is a point on the peak line. Point P_i is on the same cross-section as P_1, deviated from it at an angle α and thus the angle between O_1P_i and the x axis is $\theta_1 + \alpha$. Since the eye is so far away, the viewer can only see the overall reflectance from the visible arc. Therefore the reflected intensity is actually the average intensity over the visible arc. We first formulate the intensity of light twice reflected specularly. Consider a small arc $[\theta_1 + \alpha, \theta_1 + \alpha + d\alpha]$ starting from

P_i. Suppose its length when projected in the $\vec{E_p}$[2] direction is ΔL. If ΔI is the intensity reflected from P_i to the viewer[3], the intensity of light reflected from every point on this small arc can be assumed to be ΔI, since we are considering a very small arc. Therefore we have the following equation:

$$I_{ss} = \int_{-\alpha_{low}}^{\alpha_{up}} \frac{\Delta L}{L} \Delta I \tag{5.20}$$

where L is the length of the visible arc when projected in the $\vec{E_p}$ direction. Here $\frac{\Delta L}{L}$ serves as an averaging factor.

In equation 5.20, ΔL can be rewritten as:

$$\begin{aligned} \Delta L &= r_1(\sin(\theta_1 + \alpha + d\alpha - \theta_e) - \sin(\theta_1 + \alpha - \theta_e)) \\ &\approx r_1 \cos(\theta_1 + \alpha - \theta_e) d\alpha \end{aligned} \tag{5.21}$$

where r_1 is the radius of cylinder C_1, θ_e the angle from $\vec{E_p}$ to the x axis.

If we suppose the visible arc starts from ϕ_{inf} and ends at ϕ_{sup} when measured counter-clockwisely from the x axis direction, then the term L in equation 5.20 can be rewritten as:

$$L = r_1 * (\sin(\phi_{sup} - \theta_e) - \sin(\phi_{inf} - \theta_e)) \tag{5.22}$$

In equation 5.20, ΔI is the intensity of light coming to P_i from its adjacent cylinder and then reflected to the viewer. Consider the small region at point P_j on cylinder C_2 (figure 5.6). Its cross-section starts from P_j and ends after a small angle $\Delta\beta$, and along the y axis it begins at P_j and expands at a length of Δl. Since $\Delta\beta$ and Δl are small, the intensity of light sent from every point on this small region to P_i can be assumed to be constant, which will be referred to as I_m. Then the intensity of light reflected from this small region to P_i and then to the viewer is:

[2] $\vec{E_p}$ is the projection of $\vec{E}$ on the xz plane.

[3] Again, ΔI refers to the intensity reflected only specularly at the two points.

$$I_r = \rho_s(\vec{N}_i \cdot \vec{H}_i)^n(\vec{N}_i \cdot \vec{P_iP_j})I_m d\omega \tag{5.23}$$

where $\vec{N}_i$ is the normal vector at P_i, $\vec{H}_i$ is the bisector of $\vec{E}$ and the unit vector $\vec{P_iP_j}$, n is the the specular-reflection exponent, $d\omega$ is the the solid angle of the small region with respect to P_i.

As indicated before, I_m can be regarded as equal to the intensity sent from P_j to P_i since we are considering a very small region. This yields the following equation:

$$I_m = \rho_s(\vec{N}_j \cdot \vec{H}_j)^n I_i \tag{5.24}$$

where $\vec{N}_j$ is the the normal vector at P_j, $\vec{H}_j$ is the bisector of $\vec{L}$ and unit vector $\vec{P_jP_i}$, I_i is the the intensity of light source.

For the small area, the solid angle can be calculated as the foreshortened surface area divided by the square of the distance from P_j to P_i. Therefore $d\omega$ in equation 5.23 can be rewritten as:

$$\begin{aligned} d\omega &= (\vec{N}_j \cdot \vec{P_jP_i})dA/R^2 \\ &= (\vec{N}_j \cdot \vec{P_jP_i})r_2 d\beta dl/R^2 \end{aligned} \tag{5.25}$$

where dA is the the surface area of the small region, R is the the distance from P_j to P_i, r_2 is the radius of cylinder C_2.

Combining equations 5.23, 5.24, and 5.25, the intensity of light reflected from the small region to P_i and then to the viewer can be written as:

$$I_r = \frac{r_2}{R^2}\rho_s^2(\vec{N}_i \cdot \vec{H}_i)^n(\vec{N}_j \cdot \vec{H}_j)^n(\vec{N}_i \cdot \vec{P_iP_j})(\vec{N}_j \cdot \vec{P_jP_i})I_i d\beta dl \tag{5.26}$$

Therefore, ΔI in equation 5.20, the intensity of light reflected from its adjacent cylinder to P_i and then to the viewer is:

$$\Delta I = \int_{-\beta_{low}}^{\beta_{up}} \int_{-l_0}^{l_0} \frac{r_2}{R^2}\rho_s^2(\vec{N}_i \cdot \vec{H}_i)^n(\vec{N}_j \cdot \vec{H}_j)^n(\vec{N}_i \cdot \vec{P_iP_j})(\vec{N}_j \cdot \vec{P_jP_i})I_i d\beta dl \tag{5.27}$$

Combining equations 5.20, 5.21, and 5.27, we have:

$$I_{ss} = \rho_s^2 I_i \frac{r_2 * r_1}{L} \int_{-\alpha_{low}}^{\alpha_{up}} \int_{-\beta_{low}}^{\beta_{up}} \int_{-l_0}^{l_0} \cos(\theta_1 + \alpha - \theta_e)(\vec{N}_i \cdot \vec{H}_i)^n (\vec{N}_j \cdot \vec{H}_j)^n (\vec{N}_i \cdot \vec{P_iP_j})(\vec{N}_j \cdot \vec{P_jP_i})/R^2 d\alpha d\beta dl \quad (5.28)$$

where ρ_s is the specular-reflection coefficient, I_i is the the intensity of light source, r_1 is the the radius of cylinder C_1, r_2 is the the radius of cylinder C_2, θ_1 is the angle of maximum reflection point, θ_e is the angle from $\vec{E}_p$ to the x axis, $\vec{N}_i$ is the normal vector at P_i, $\vec{H}_i$ is the bisector of $\vec{E}$ and the unit vector $\vec{P_iP_j}$, n is the the specular-reflection exponent, $\vec{N}_j$ is the normal vector at P_j, $\vec{H}_j$ is the bisector of $\vec{L}$ and the unit vector $\vec{P_jP_i}$, R is the the distance from P_i to P_j.

Similarly, for the light reflected first specularly then diffusely, the final intensity reflected to the viewer is:

$$I_{sd} = \rho_s \rho_d I_i \frac{r_2 * r_1}{L} \int_{-\alpha_{low}}^{\alpha_{up}} \int_{-\beta_{low}}^{\beta_{up}} \int_{-l_0}^{l_0} \cos(\theta_1 + \alpha - \theta_e)(\vec{N}_i \cdot \vec{P_iP_j})^2 (\vec{N}_j \cdot \vec{H}_j)^n (\vec{N}_j \cdot \vec{P_jP_i})/R^2 d\alpha d\beta dl \quad (5.29)$$

the intensity of light reflected first diffusely then specularly to the viewer is:

$$I_{ds} = \rho_s \rho_d I_i \frac{r_2 * r_1}{L} \int_{-\alpha_{low}}^{\alpha_{up}} \int_{-\beta_{low}}^{\beta_{up}} \int_{-l_0}^{l_0} \cos(\theta_1 + \alpha - \theta_e)(\vec{N}_i \cdot \vec{H}_i)^n (\vec{N}_j \cdot \vec{L}) (\vec{N}_i \cdot \vec{P_iP_j})(\vec{N}_j \cdot \vec{P_jP_i})/R^2 d\alpha d\beta dl \quad (5.30)$$

the intensity of light reflected diffusely twice is:

$$I_{dd} = \rho_d^2 I_i \frac{r_2 * r_1}{L} \int_{-\alpha_{low}}^{\alpha_{up}} \int_{-\beta_{low}}^{\beta_{up}} \int_{-l_0}^{l_0} \cos(\theta_1 + \alpha - \theta_e)(\vec{N}_i \cdot \vec{P_iP_j})^2 (\vec{N}_j \cdot \vec{L}) (\vec{N}_j \cdot \vec{P_jP_i})/R^2 d\alpha d\beta dl \quad (5.31)$$

As discussed before, we integrate the reflected intensities over the regions surrounding the maximum reflection point P_i and the peak line because in this way we will not miss the peak reflectance and will ensure quick convergence of the result. Consequently, the

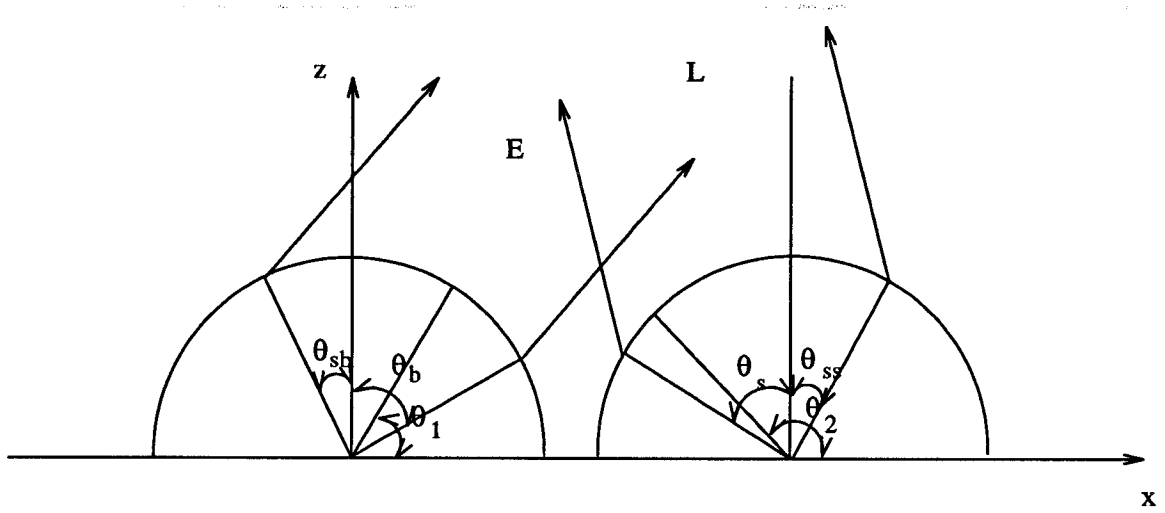

Figure 5.7: Additional Constraints for the Integration Range

regions being integrated can be minimized. When we formulate the secondary reflection, we assume that any point in the integrated region on C_1 is visible to all of the points in the integrated region on C_2. This is another reason why we have to minimize $\alpha_{up}, \alpha_{low}, \beta_{up}, \beta_{low}$. In practice, we constrain them by a small constant C_{max}. In any case, it is sufficient if C_{max} is chosen as 0.3. Normally, a value of 1.5 is enough for l_0, since distance is another crucial attenuation factor in our formula. In addition, we have to ensure that the integrated region on cylinder C_1 is visible to the viewer and the region on C_2 is illuminated by the light source. Another constraint is that α_{up} and β_{low} be small enough so that any region under integration stays in only one side of the z axis (figure 5.7). Finally, $\alpha_{up}, \alpha_{low}, \beta_{up}$ and β_{low} are determined by the following pseudocode:

```
if ( EX same side) {
      αup = min(π/2 − θ1, Cmax);
      αlow = min(θb − (π/2 − θ1), Cmax); }
else {
      αup = min(π/2 − θ1, Cmax);
      αlow = min(θsb + θ1 − π/2, Cmax); }
```

```
if ( LX same side ) {
```
$\beta_{up} = min(C_{max}, \theta_{ss} - (\theta_2 - \pi/2));$
$\beta_{low} = min(C_{max}, \theta_2 - \pi/2);$ }
```
else {
```
$\beta_{up} = min(C_{max}, \theta_s - (\theta_2 - \pi/2));$
$\beta_{low} = min(C_{max}, \theta_2 - \pi/2);$ }

For the case that P_1 on the other side of the z axis, the calculation is:

```
if ( EX same side ) {
```
$\alpha_{up} = min(\theta_{sb} - (\theta_1 - \pi/2), C_{max});$
$\alpha_{low} = min(\theta_1 - \pi/2, C_{max});$ }
```
else {
```
$\alpha_{up} = min(\theta_b - (\theta_1 - \pi/2), C_{max});$
$\alpha_{low} = min(\theta_1 - \pi/2, C_{max});$ }
```
if ( LX same sside ) {
```
$\beta_{up} = min(C_{max}, \pi/2 - \theta_2);$
$\beta_{low} = min(C_{max}, \theta_s - (\pi/2 - \theta_2));$ }
```
else {
```
$\beta_{up} = min(C_{max}, \pi/2 - \theta_2);$
$\beta_{low} = min(C_{max}, \theta_{ss} - (\pi/2 - \theta_2));$ }

At the current stage, we have not found a more easily integrable formulation of the secondary reflection, and we have not been able to closely approximate the terms under integration by some polynomial or other easily integrated form. In our current implementation, we use numerical integration, specifically Simpson's *Adaptive Quadrature Method* [Burd81] to evaluate the integrals.

5.4 Result

We have presented the raytracing and analytical solution to the secondary reflection problem. Initially, to have some degree of verification, we will compare the results from the two approaches. We rendered a sphere using each of the two approaches. We chose a sphere since it can represent a wide range of parameters. The sphere is centered at (0,0,0). The light source is in the direction of (0, -0.5, 0.87), the eye is at (0, -10, 10).

The material property of the sphere is: $\rho_d = 0.4, \rho_s = 0.7, n = 1$. The anisotropy of the sphere is modeled as longitudinal cylinder group with parameters $d = 2, r = 1, h = 0$. We rendered the sphere using the two solutions separately and for each of them, we recorded the direct specularly reflected intensity I_s and the secondary specularly reflected intensity I_{ss} of every pixel on the sphere. In figure 5.8, for each of these pixels, a point is plotted with the recorded I_s as its x coordinate and I_{ss} as its y coordinate. The data from the raytracing solution are plotted in red and those from the analytical solution are in green. Figure 5.9 is plotted similarly except that the y coordinate is the ratio of I_{ss} and I_s instead of I_{ss}. From the two figures one can see that the results from the two solutions are very similar. The small difference might be caused by the fact that, in our analytical solution, part of the cylinders are truncated for numerical integration. We are convinced in some degree that the two solutions are correct.

Our initial goal was to calculate the secondary reflection and compare it to the direct reflection. Next, we will show the comparison numerically as well as visually. The results presented in the following are from the analytical solution. We rendered a disk residing on the $z = 0$ plane. The directional light source is 75° with the $z = 0$ plane and the eye is at (0, -10, 10). The material property of the disk is: $\rho_d = 0.4, \rho_s = 0.7$, with different n's for different scenes. The anisotropy of the disk is modeled with longitudinal cylinders with parameters $d = 2, r = 1, h = 0$. For each scene in figure 5.10, the disk is shaded with only secondary specular reflection I_{ss}. In figure 5.11, the disk is shaded with the overall secondary reflection I_2 (i.e. $I_{ss} + I_{sd} + I_{ds} + I_{dd}$). From these two pictures, one can perceive how the secondary reflection changes when n varies. As our numerical results, we will compare I_{ss} with direct specular reflection I_s and I_2 with the overall direct reflection I_1 (i.e. $I_s + I_d$). Again, this is presented in the form of a point plot with the intensity of direct reflection as x coordinate and the intensity of secondary reflection as y coordinate. Figure 5.12 compares I_{ss} and I_s. Figure 5.13 compares I_2 and I_1. For

different n's, the points are plotted in different colours.

Figure 5.14 depicts the distributions of the four components I_{ss}, I_{sd}, I_{ds} and I_{dd} of I_2 for various n's. Table 5.2 summarizes the numerical results. It lists for different n's the maximum I_{ss}, maximum I_{ss}/I_s, maximum I_2 and maximum I_2/I_1. Based on table 5.2, we plot points with n (column 1 in the table) as its horizontal coordinate and maximum I_2 (column 4 in the table) as its vertical coordinate in figure 5.15. We then connect these points in order of increasing n to form a polyline. We plot figure 5.16 similarly with n as the horizontal coordinate and the maximum ratio I_2/I_1 (column 5 in table 5.2) as the vertical coordinate. It should be noted that in figure 5.15 and 5.16, the horizontal and the vertical axes are drawn at different scales. The information conveyed in these two graphs gives us a good visualization of how the secondary reflected intensity changes when n varies for a typical scene. However, it should be pointed out that all the data in table 5.2 and figures 5.15 and 5.16 are from a specific scene. When the object, $\vec{L}$ or $\vec{E}$ change, we anticipate different proportions.

From the above results, one can see that when n is small (less than 8 to 12), I_{ss} and I_2 are very strong. Among the four components of I_2, I_{ss} is the most important component. However, when n increases, its weight decreases sharply, but the I_{dd} term increases its relative contribution. The distributions of I_{sd} and I_{ds} are fairly stable but still increase slightly as n increases. When n is greater than 16, the term I_{ss} becomes very small. However, the overall reflection I_2 is still impressive. When n lies in this range, the term I_{dd} becomes the heaviest component, I_{sd} the next, I_{ss} the least. When n becomes even larger (greater than 35), I_2 and I_2/I_1 are very small and tends to be stable. This is because its most significant component I_{dd} does not change as n changes. Therefore when $n > 35$, I_2 can be neglected although it is still noticeable, since the computation of secondary reflection is very expensive. It takes about 3 to 4 hours to render a scene as simple as a single disk. To summarize the results presented here, we conclude that

n	maximum I_{ss}	maximum I_{ss}/I_s	maximum I_2	maximum I_2/I_1
1	0.207819	0.362343	0.469707	0.533371
2	0.164824	0.323570	0.412178	0.506787
4	0.117699	0.273994	0.332843	0.462316
8	0.071946	0.230949	0.246033	0.399570
12	0.050398	0.204543	0.200293	0.356872
16	0.038186	0.184313	0.171976	0.327919
20	0.030145	0.175941	0.152782	0.305521
24	0.024738	0.124271	0.138825	0.288425
32	0.016490	0.111017	0.118240	0.261176
40	0.011692	0.266447	0.106005	0.246188
55	0.009911	0.262630	0.093535	0.228236
70	0.007606	0.286665	0.084388	0.220936
90	0.007606	0.286665	0.084388	0.220936

Table 5.2: Maximum Values for different specular exponents

the secondary reflection shows strong anisotropy and it can not be simply approximated by the diffuse term in traditional lighting models. When n is small (less than 20), the secondary reflected intensity is quite strong and not negligible. When n is large (greater than 35), the secondary reflected intensity is very small and thus can be neglected due to the computational expense. When n is inbetween, accuracy and speed requirements becomes important.

For cloth surfaces, normally the specular exponent n is relatively small (between 6 and 15). Therefore the inter-reflection should be taken into consideration. Due to the local geometry of the cloth surface, the inter-reflection consists of two elements: inter-reflected intensity from parallel cylinder segments and that from perpendicular cylinder segments. We use raytracing to test and compare these two elements and find out that inter-reflected intensity from perpendicular cylinder segments seldom exceeds a quarter of the inter-reflected intensity from parallel cylinder segments. Thus we conclude that if we

disregard the inter-reflection between perpendicular cylinder segments, and approximate the total inter-reflection by the inter-reflection between parallel cylinder segments, the error will not be intolerable. The following pictures in figure 5.17 are rendered with the analytical solution accounting for inter-reflection. It corresponds to figure 4.5 in chapter 4; the four scenes are in the same order and the object, light and eye for each scene are the same. We can see that the pictures with inter-reflection look more realistic. However, this is offset by a longer rendering time. Previously about 10 minutes was required to render each of the four pictures without inter-reflection. For the four with inter-reflection, about 40 minutes are required for each.

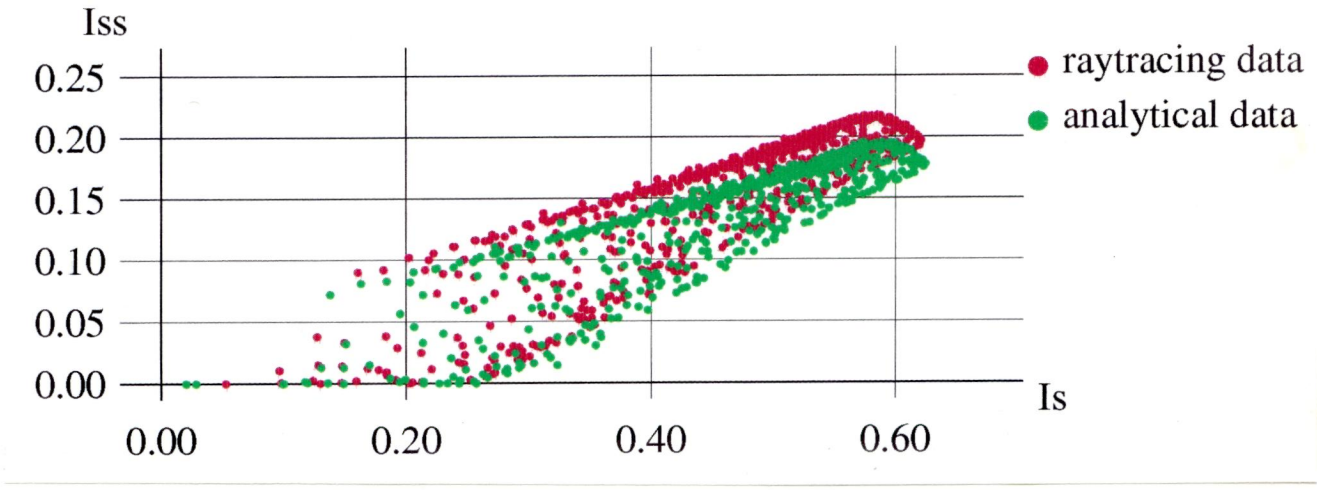

Figure 5.8: Numerical Comparison of Raytracing and Analytical Solution (I_{ss} vs. I_s)

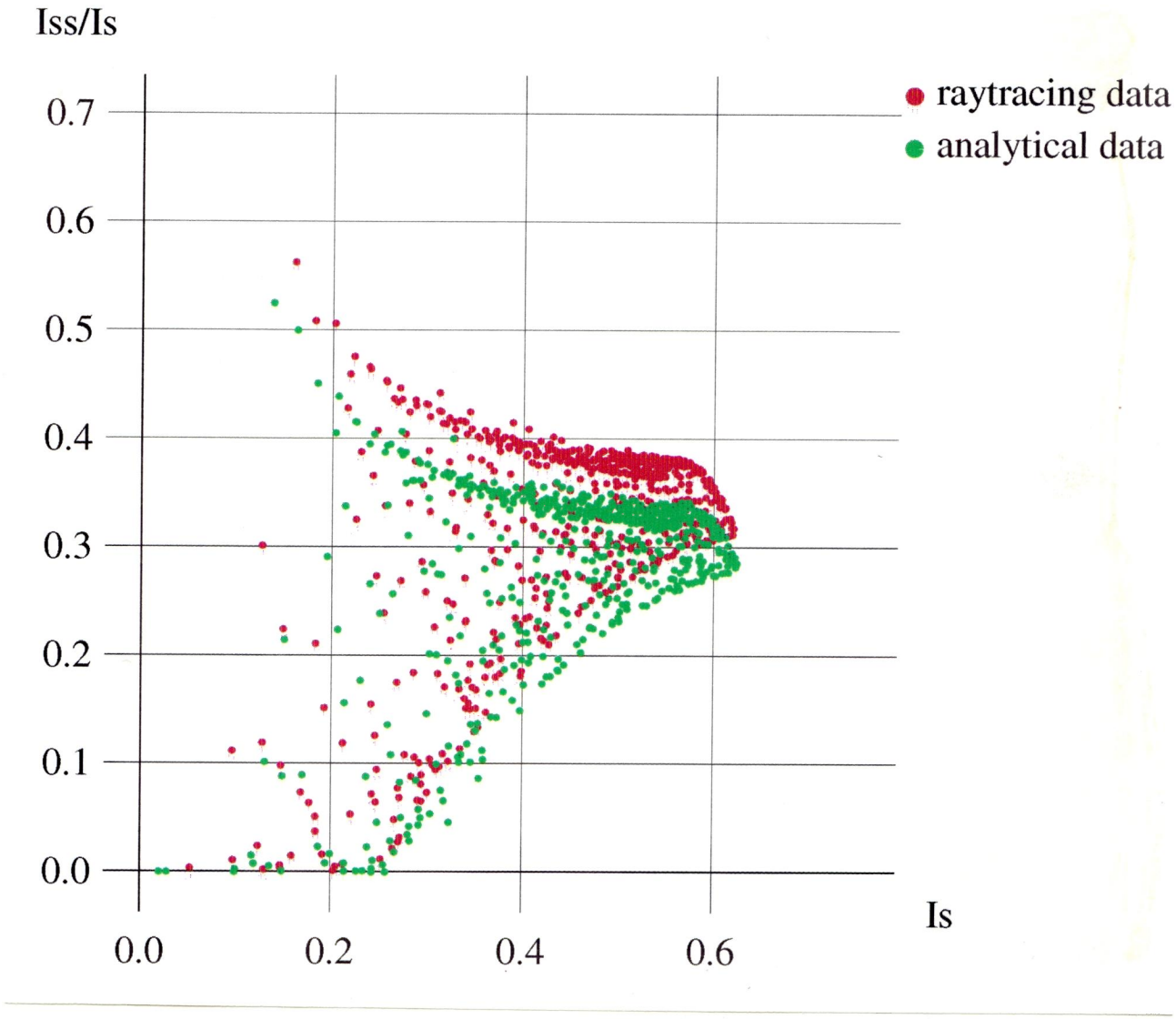

Figure 5.9: Numerical Comparison of Raytracing and Analytical Solution (I_{ss}/I_s vs. I_s)

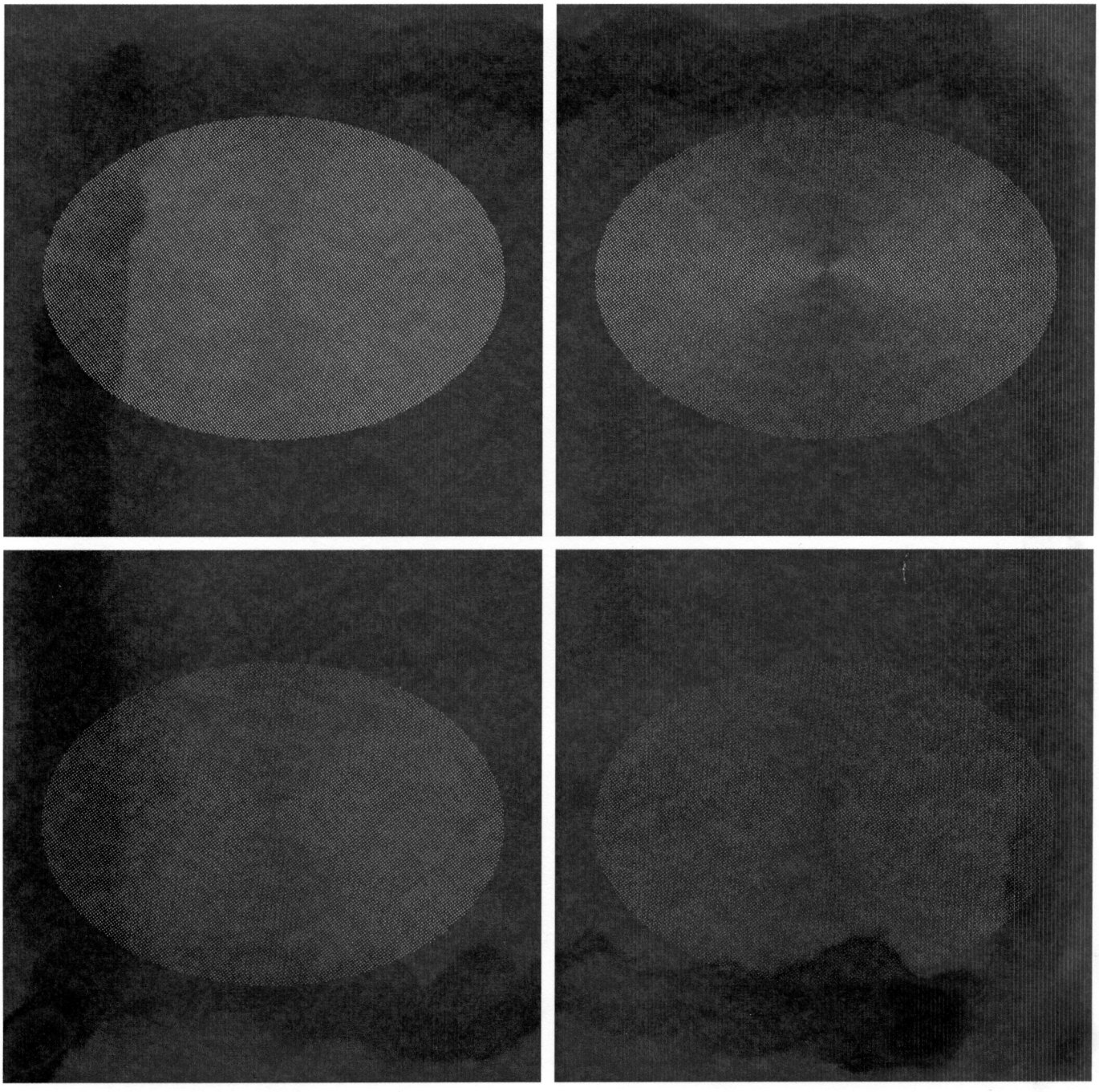

1	2
3	4

Image 1: n =1; Image 2: n=2; Image 3: n=4; Image 4: n=8;

Figure 5.10: A Disk Shaded with Specular Secondary Reflection I_{ss} for various specular exponents (to be continued)

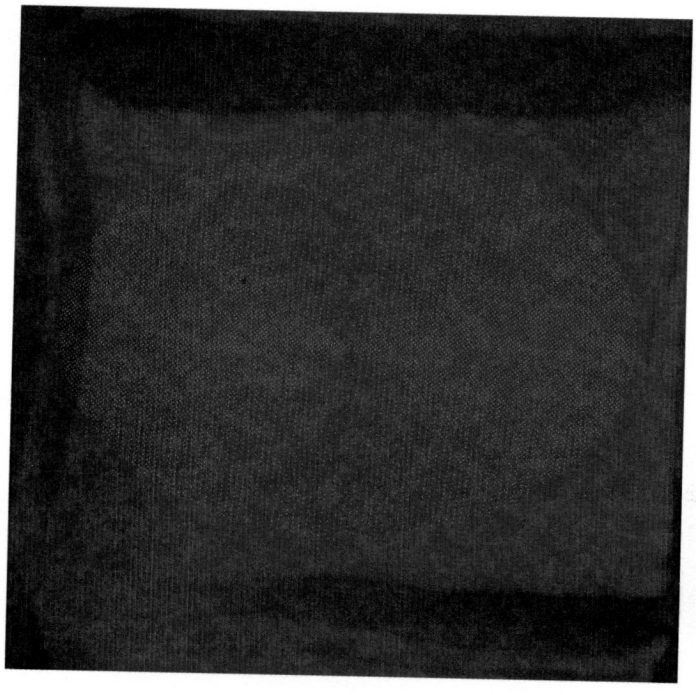

5

Image 5: n =16.

Figure 5.10: A Disk Shaded with Specular Secondary Reflection I_{ss} for various specular exponents (continued)

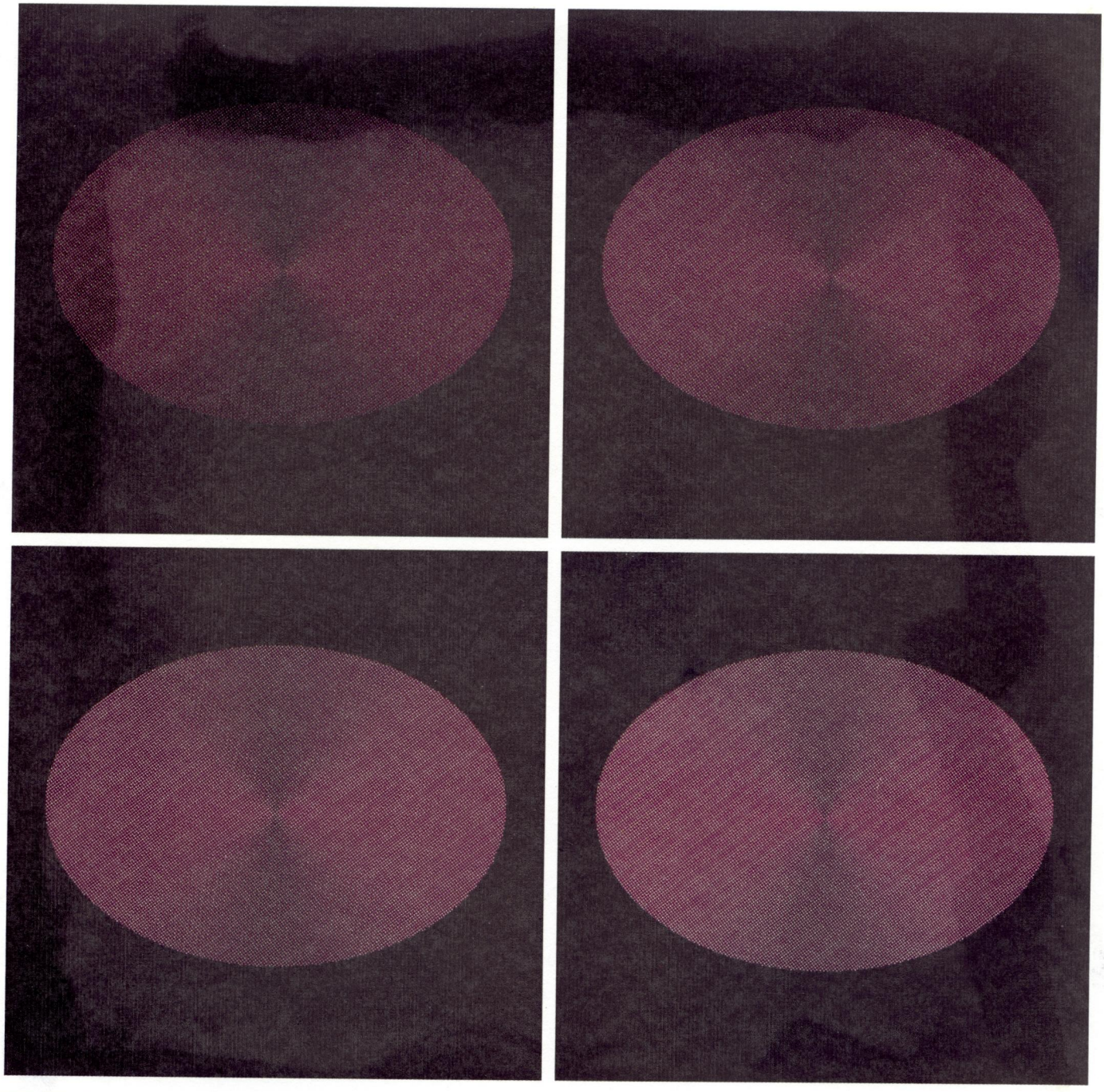

1	2
3	4

Image 1: n =1; Image 2: n=2; Image 3: n=4; Image 4: n=8;

Figure 5.11: A Disk Shaded with Overall Secondary Reflection I_2 for various specular exponents (to be continued)

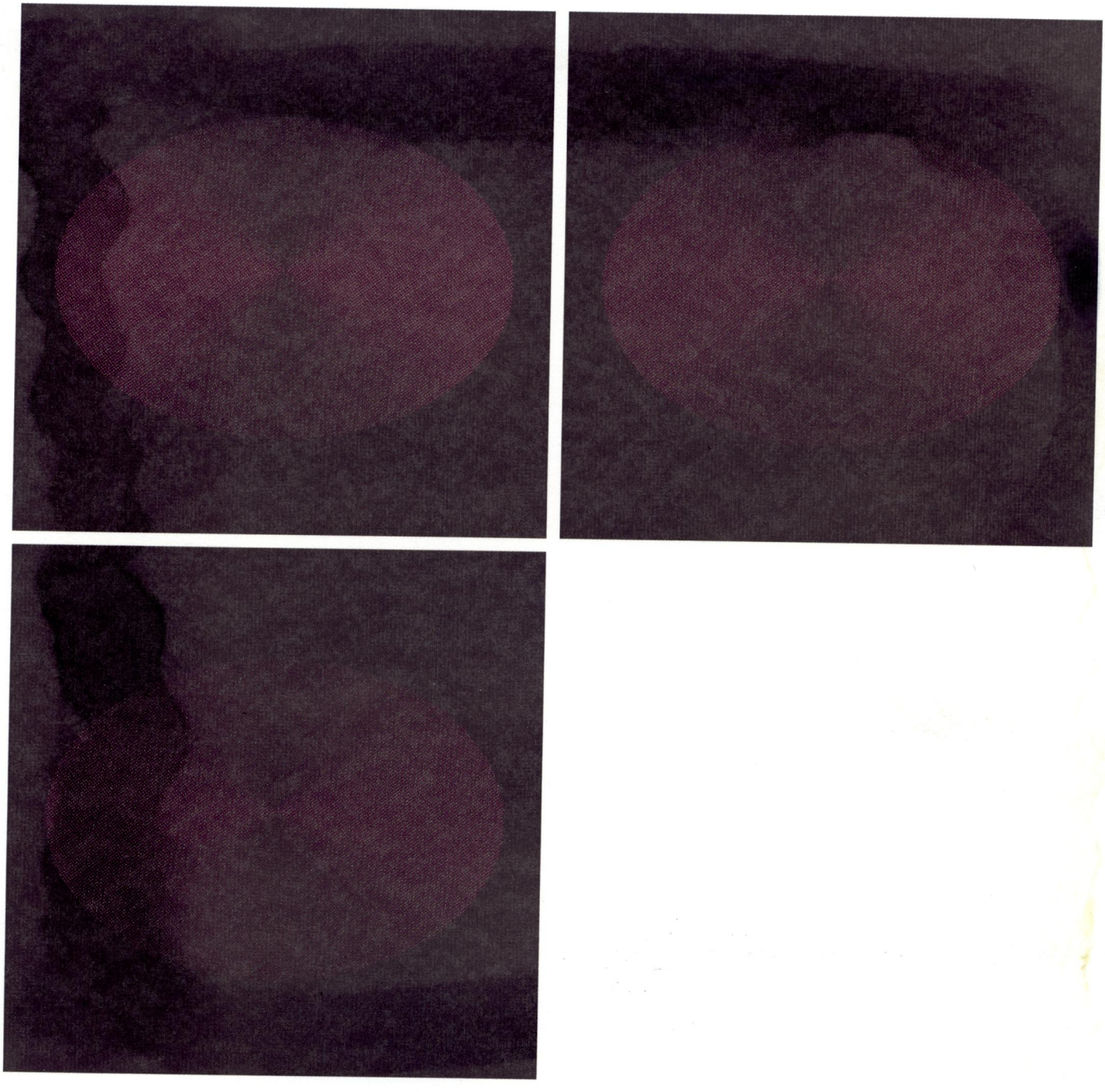

5	6
7	

Image 5: n =16; Image 6: n=24; Image 7: n=32.

Figure 5.11: A Disk Shaded with Overall Secondary Reflection I_2 for various specular exponents (continued)

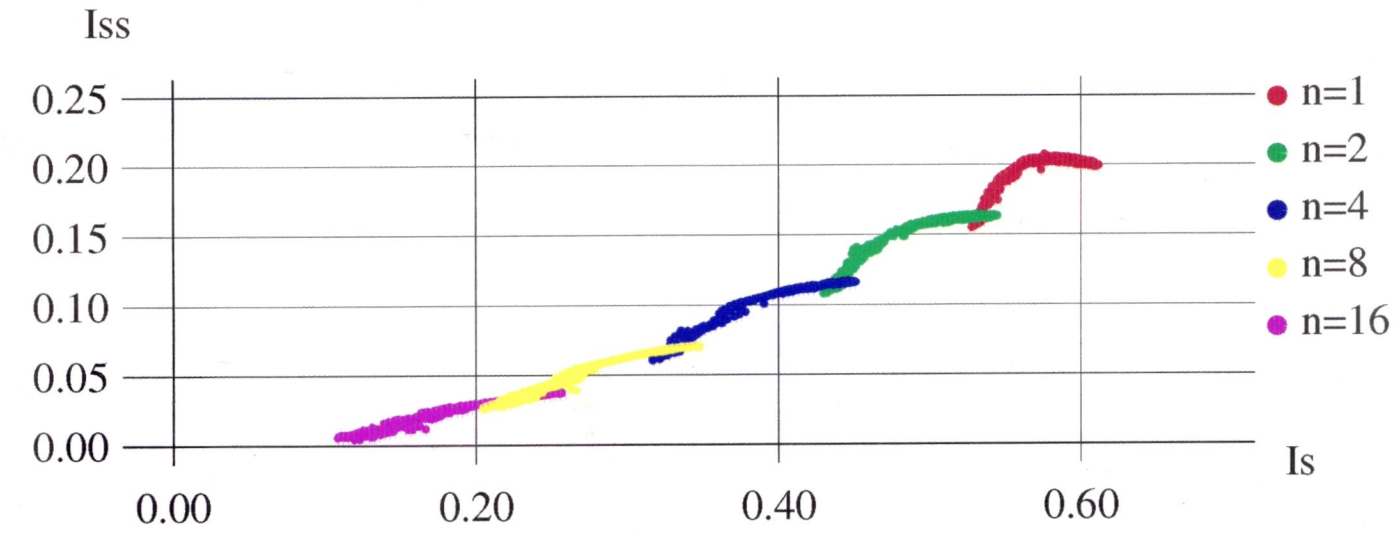

Figure 5.12: Numerical Comparison of I_{ss} and I_s for various specular exponents

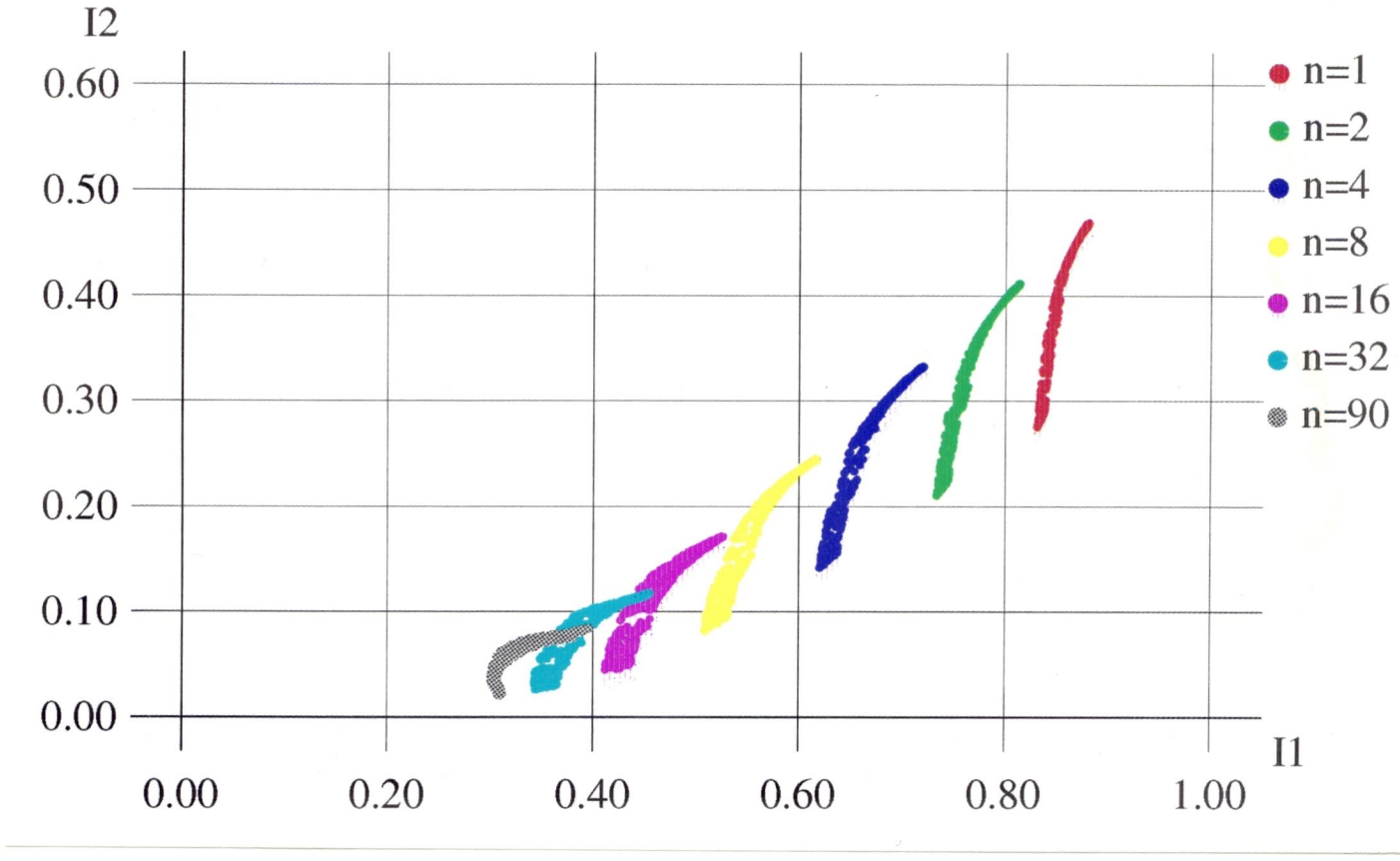

Figure 5.13: Numerical Comparison of I_2 and I_1 for various specular exponents

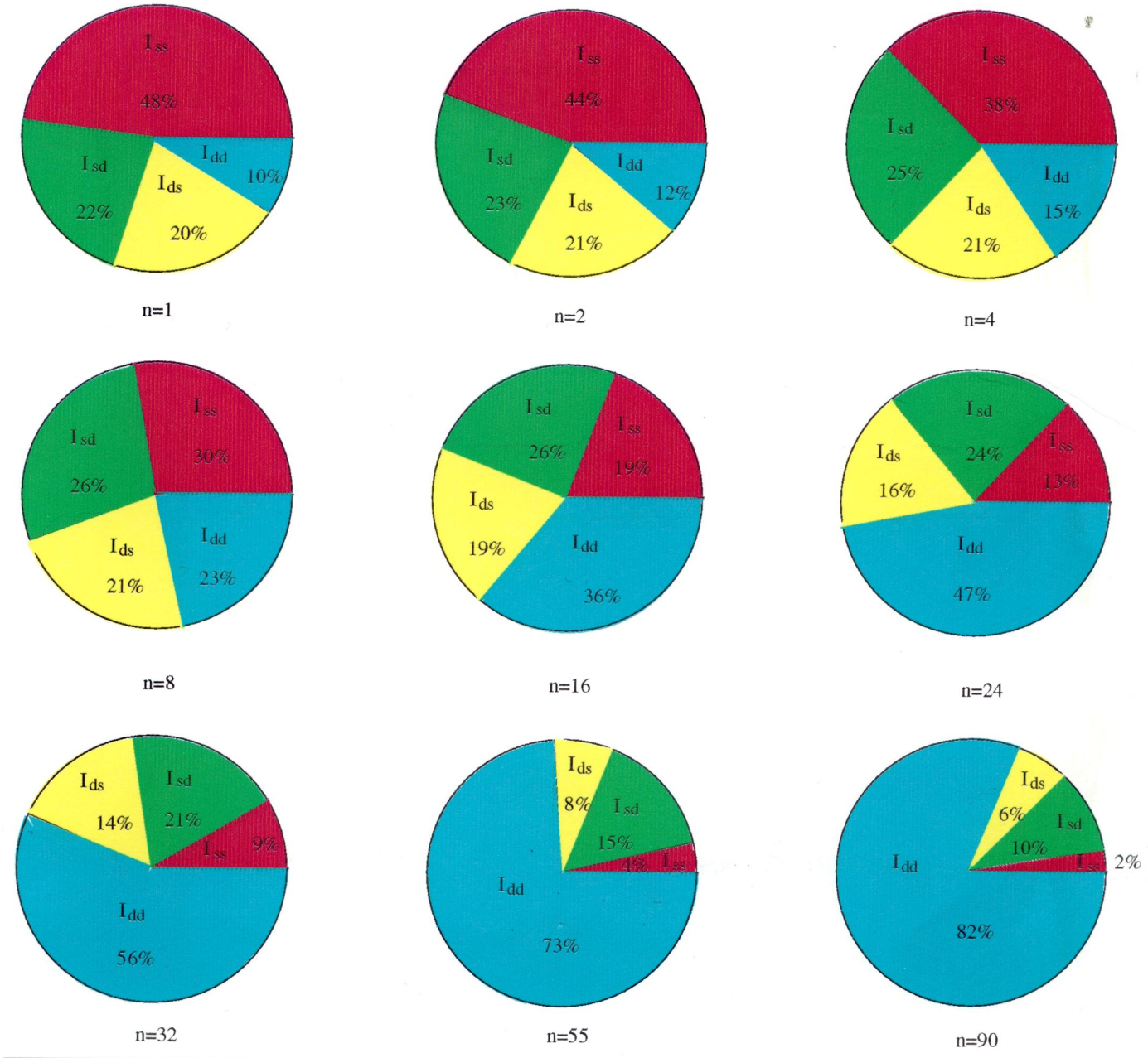

Figure 5.14: Distributions of I_{ss}, I_{sd}, I_{ds} and I_{dd} in I_2 for Various specular exponents

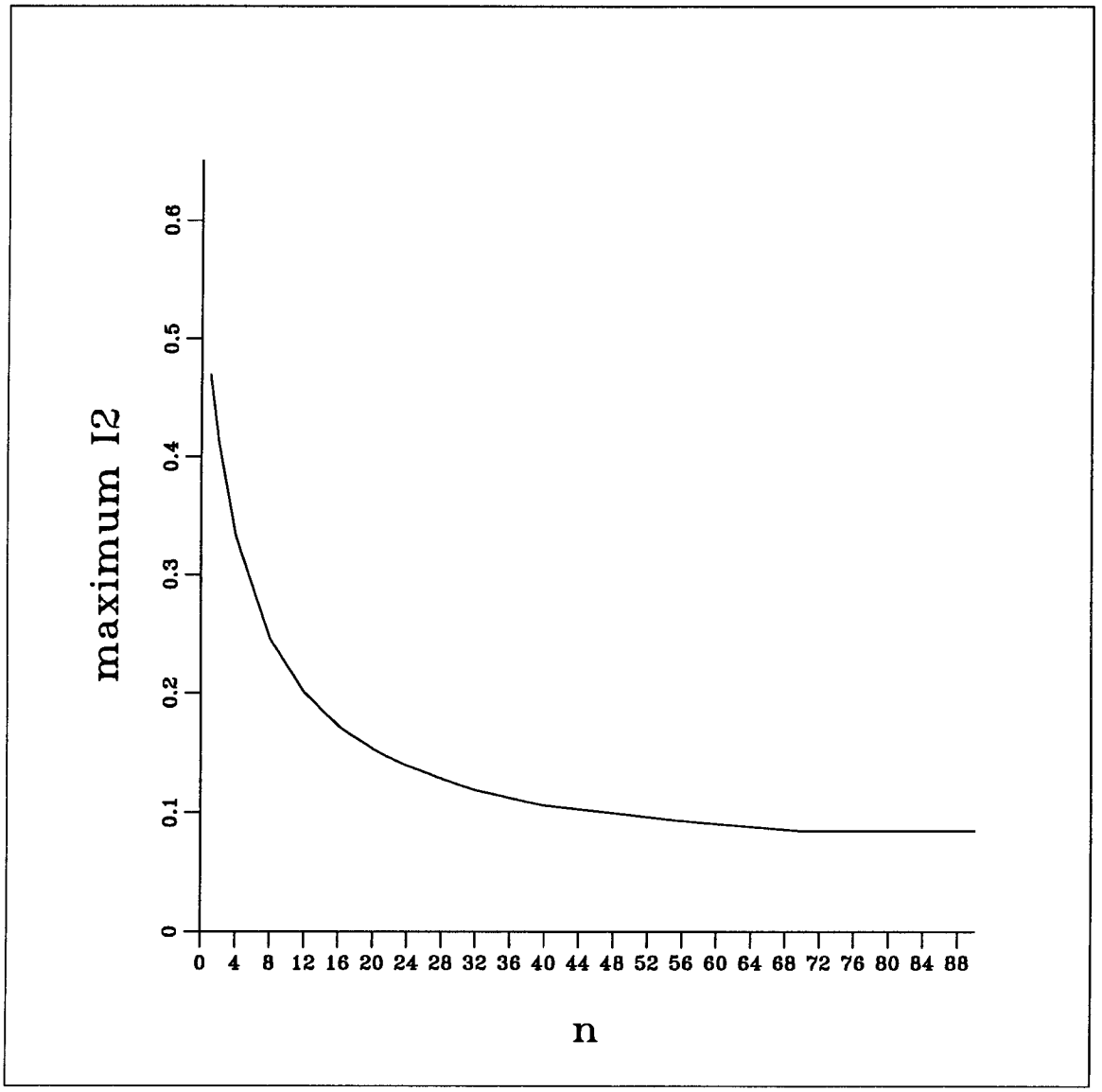

Figure 5.15: Variation of Secondary Reflection with Respect to specular exponent

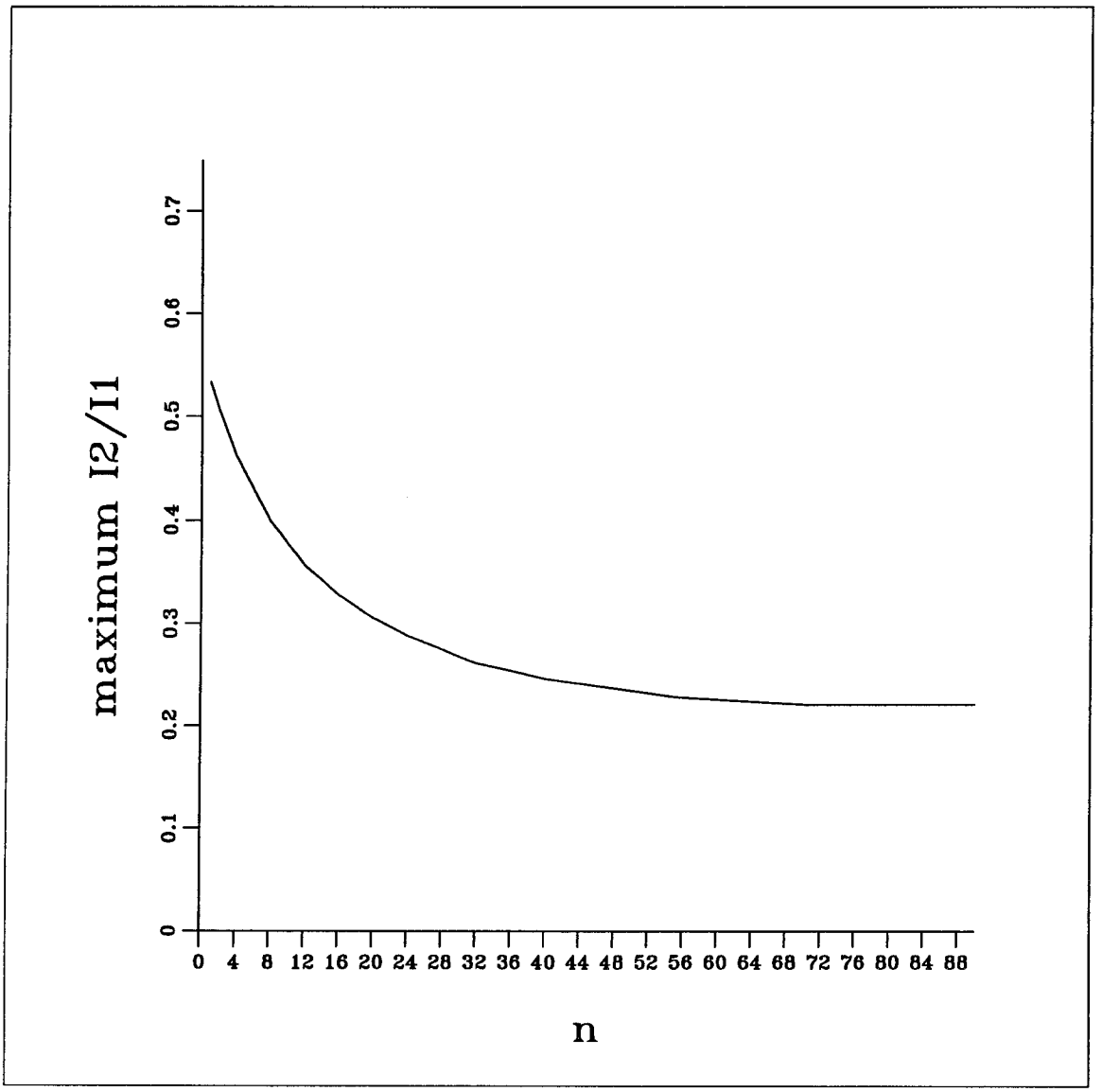

Figure 5.16: Variation of I_2/I_1 with Respect to specular exponent

1	2
3	4

Image 1: basket weave (eye at (0, -55, 45)); Image 2: basket weave (eye at (-45, 45, 80));
Image 3: twill weave (eye at (0, -55, 45); Image 4: twill weave (eye at (-45, 45, 80)).

Figure 5.17: Sample Cloth Images with Inter-reflection Accounted

Chapter 6

Conclusion and Future Work

In this thesis, we propose a model to simulate the small-scale geometry of cloth and a method to derive the BRDF (Bidirectional Reflectance-Distribution Function) of this model from the underlying surface geometry, taking into account the blocking and shadowing phenomena at the small scale. Sample images of cloth generated with this BRDF look highly realistic. As a starting point to the inter-reflection problem, we examine the secondary reflection phenomena for the surface model made of parallel cylinders (as proposed by Poulin and Fournier in [Poul89] [Poul90]) and the model proposed here for cloth. We assume the facets composing the cylinders as phong-like model. Two solutions are presented — sampling through raytracing and an analytical approximation. The result convinces us that the multiply reflected intensity could be substantial for bumped surfaces with low specular exponent n (less than 20). Therefore inter-reflection should be accounted for in the lighting model for these surfaces. Generated cloth images with secondary reflection effects included exhibit a higher degree of realism. However, the computation of secondary reflection effects is quite expensive. For some scenes, the additional cost is several times of that required for computing the direct reflection.

The techniques presented can be extended to extract macroscopic reflection behaviour from the knowledge of the microscopic geometric structure.

For the inter-reflection, there are still many possible extensions and additional works for the problem. First of all, a faster computation is highly desired for the analytical

solution. The convergence of the inter-reflection is still unknown. Given that raytracing will be expensive, can we find an analytical solution? In this thesis, we have only examined the secondary reflection on some specific surface models. The inter-reflection phenomena on different surface geometries (including regular and random) need further investigation. In our solutions for secondary reflection problem, we assume that the micro-facets composing the cylinders are phong model. As shown in [Lewi93], phong model does not satisfy the physical constraints of energy conservation and Helmholtz reciprocity. It will be physically more plausible if we assume that the facets are those models that conserve energy and satisfy reciprocity. It will also be interesting to see the difference in the rendered results when different models are applied.

The approaches presented in this thesis are implemented in a raytracing systems called "optik". How to integrate these algorithms into large rendering software is challenging. In addition, the integration of these approaches into global illumination systems requires additional works. We have to adjust our algorithms to make sure they fulfill all the necessary physical constraints.

There is another issue that needs to be addressed, i.e. hierarchy of models. In some circumstances, only one intermediate level between the macroscopic and the microscopic level will not be enough. For example, when one looks at a desert[1] from an airplane, each grain of sand can be thought of comprising the lowest level, or the micro-facets. The character of these facets could be described by the traditional lighting models in computer graphics. The next higher level corresponds to the scale of grains of sand. The third level, which corresponds to the pixel level, is the level with scale equivalent to small sand dune. The highest level is the geometric shape of the large region. In this situation, there are two levels between the microscopic and macroscopic level. Two possible approaches exist. One is to examine all of the four levels from the bottom up to the top, with the full

[1]Of course, we assume it is not cloudy.

cost associated with this. The alternative is to first find a good BRDF for the level right below the pixel level, and thereafter simplify the multiple intermediate levels to only a single intermediate level.

Yes, still have a long way to go .....

Bibliography

[ANS86] American National Standard, *Nomenclature and Definitions for Illuminating Engineering.* Illuminating Engineering Society of North America, 1986.

[Bass79] F. G. Bass, and I. M. Fuks. *Wave Scattering from Statistically Rough Surfaces.* Pergamon Press Ltd., 1979.

[Beck63] P. Beckmann, and A. Spizzichino. *The Scattering of Electromagnetic Waves from Rough Surfaces.* Pergamon, Oxford 1963.

[Blin77] J. Blinn. Models of Light Reflection for Computer Synthesized Pictures, *Computer Graphics*, Vol. 11, No. 2, July 1977, pp. 192-198.

[Blin78] J. Blinn. Simulation of Wrinkled Surfaces, *Computer Graphics*, Vol. 12, No. 3, August 1978, pp. 286-292.

[Born75] M. Born, and E. Wolf. *Principles of Optics.* Pergamon, Oxford, 1975.

[Burd81] R. L. Burden, J. D. Faires, and A. C. Reynolds. *Numerical Analysis.* Second Edition, PWS Publishers, Boston, Massachusetts, 1981.

[Cabr87] B. Cabral, N. Max, and R. Springmeyer. Bidirectional Reflection Functions from Surface Bump Maps, *Computer Graphics*, Vol. 21, No. 4, July 1987, pp. 273-281.

[Cook81] R. Cook, and K. Torrance. A Reflection Model for Computer Graphics, *Computer Graphics*, Vol. 15, No. 3, August 1981, pp. 307-316. Also in *ACM Transactions on Graphics*, Vol. 1, No. 1, January 1982, pp. 7-24.

[Corb79] B. P. Corbman. *Textiles: Fiber to Fabric.* Canadian Edition. McGraw-Hill, 1979.

[Four92] A. Fournier. Normal Distribution Functions and Multiple Surfaces, Proceedings of Graphics Interface'92, In *Workshop on Local Illumination* (May 1992), pp. 45-52.

[Gart92] J. A. Gartaganis. A Wave-based Illumination Model for Computer Graphics, Ph.D thesis, Department of Computing Science, University of Alberta 1992.

[Hall83] R. A. Hall, and D. P. Greenberg. A Testbed for Realistic Image Synthesis, *IEEE Computer Graphics and Applications* Vol. 3, No. 8, November 1983, pp. 10-20.

[Hall89] R. A. Hall. *Illumination and Color in Computer Generated Imagery.* Springer-Verlag, 1989.

[He91] X. He, K. E. Torrance, F. X. Sillion, and D. P. Greenberg. A Comprehensive Physical Model for Light Reflection, *Computer Graphics*, Vol. 25, No. 4, July 1991, pp. 175-186.

[Kaji85] J. T. Kajiya. Anisotropic Reflection Models, *Computer Graphics*, Vol. 19, No. 3, July 1985, pp. 15-21.

[Lewi93] R. R. Lewis. Making Shaders More Plausible, submitted to *4th Eurographics Conference on Rendering*, June 1993.

[Max88] N. Max. Horizon Mapping: Shadows for Bump-Mapped Surfaces, *The Visual Computer*, Vol. 4, 1988, pp. 109-117.

[Minn41] M. Minnaert. The Reciprocity Principle in Lunar Photometry, *Astrophysical Journal*, Vol. 93, May 1941, pp. 403-410.

[Neum89] L. Neumann, and A. Neumann. Photosimulation: Interreflection with Arbitrary Reflectance Models and Illumination, *Computer Graphics Forum*, Vol. 8, No. 1, March 1989, pp. 21-34.

[Phon73] B. Phong. Illumination for Computer Generated Pictures, *Communications of ACM*, Vol. 18, No. 6, June 1975, pp. 311-317.

[Pizz61] J. J. Pizzuto. *101 Weaves in 101 Fabrics.* Textile Press, 1961.

[Pizz87] J. J. Pizzuto. *Fabric Science.* Fifth Edition, Fairchild Publications, 1987.

[Poul89] P. Poulin. Anisotropic Reflection Models, M.Sc thesis, Department of Computer Science, University of Toronto 1989.

[Poul90] P. Poulin, and A. Fournier. A Model for Anisotropic Reflection, *Computer Graphics*, Vol. 24, No. 4, August 1990, pp. 273-282.

[Sieg81] R. Siegel, and J. Howell. *Thermal Radiation Heat Transfer,* Second Edition, Hemisphere, 1981.

[Tail92] F. Taillefer. Fast Inverse Displacement Mapping and Shading in Shadow, Proceedings of Graphics Interface'92, In *Workshop on Local Illumination* (May 1992), pp. 53-60.

[Torr67] K. Torrance, and E. Sparrow. Theory of Off-specular Reflection from Roughed Surfaces, *Journal of the Optical Society of America*, Vol. 57, No. 9, September 1967, pp. 1105-1114.

[Tort87] P. G. Tortora. *Understanding Textiles.* Third Edition, Macmillan, 1987.

[Trow75] T. Trowbridge, and K. Reitz. Average Irregularity Representation for a Roughed Surface for Ray Reflection, *Journal of the Optical Society of America*, Vol. 65, No. 5, May 1975, pp. 531-536.

[West92] S. H. Westin, J. R. Arvo, and K. E. Torrance. Predicting Reflectance Functions from Complex Surfaces. *Computer Graphics*, Vol. 26, No. 2, July 1992, pp. 255-264.

[Wing84] I. B. Wingate, and J. F. Mohler. *Textile Fabrics and Their Selection.* Eighth Edition, Prentice-Hall, 1984.

[Yasu92] T. Yasuda, S. Yokoi, J. Toriwaki, and K. Inagaki. A Shading Model for Cloth Objects, *IEEE Computer Graphics and Applications*, Vol. 12, No. 6, November 1992, pp. 15-24.